FIBERGLASS COMPOSITE TENSILE FATIGUE RESISTANCE: FIBER SURFACE DAMAGE ANALYSIS AND FATIGUE RESISTANT FIBER COATING

by

Jinhua Bian

A thesis submitted in partial fulfillment of the requirements for the degree

of

Master of Science

in

Chemical Engineering

MONTANA STATE UNIVERSITY-BOZEMAN
Bozeman, Montana

July 1996

APPROVAL

of a thesis submitted by

Jinhua Bian

This thesis has been read by each member of the thesis committee and has been found to be satisfactory regarding content, English usage, format, citations, bibliographic style, and consistency, and is ready for submission to the College of Graduate Studies.

Date

Chairperson, Graduate Committee

Approved for the Major Department

Date

Head, Major Department

Approved for the College of Graduate Studies

Date

Graduate Dean

STATEMENT OF PERMISSION TO USE

In presenting this thesis in partial fulfillment of the requirements for a master's degree at Montana State University, I agree that the Library shall make it available to borrowers under the rules of the Library.

If I indicated my intention to copyright this thesis by including a copyright notice page, copying is allowable only for scholarly purposes, consistent with "fair use" as prescribed in the U.S. Copyright Law. Requests for permission for extended quotation from or reproduction of this thesis in whole or in parts may be granted only by the copyright holder.

_____

Signature

_____

Date

ACKNOWLEDGMENT

It would be impossible to acknowledge all of the people who have contributed to this thesis.

In particular, I would like to thank Dr. John Mandell for his guidance, support and encouragement. Without his expertise, insight, this work would have taken longer.

I would also like to thank Dr. John Sears, Dr. Bonnie Tyler, and Dr. Doug Cairns for their kind guidance and serving on my committee. I also thank Dan Samborsky, experiment specialist in our group, for his help in training me and his effort to keep the facility in good condition.

Thanks are extended to following people. To James Tomposon, who ran most of the AFM tests with me. To Dongrui Fang, who carried out the XPS analysis for me. To Nancy Equall of the Imaging and Chemical Analysis Laboratory at MSU, for her assistance with SEM work. To the staff of the Chemical Engineering Department at MSU, for their help and friendship.

Thanks are also extended to Department of Energy and State of Montana for their support under DOE EPSCoR program..

This thesis is dedicated to my wife who has been waiting for this for a long time.

TABLE OF CONTENTS

	Page
1. INTRODUCTION	1
2. BACKGROUND	3
General Fatigue Properties	3
Fatigue of Metals	3
Fatigue of Polymers	4
Fatigue of Composites	6
Fatigue Behavior of Glass Fiber Reinforced Composites	8
Analysis of Composite Interface	11
Imaging of Fiber Surfaces	11
The Effect and Characterization of Composite Interface Strength	13
Characterization of Fatigue Strength	15
3. EXPERIMENTAL METHODS	16
Coating of Strands and Fabrics	16
Graphic Flake Coating Mixture	16
Fiber Coating	16
Atomic Force Microscope	17
Specimen Design	17
Test Apparatus	17
Test Procedure	18
Microdebonding Test	19
Specimen Preparation	20
Test Procedure	21
Scanning Electron Microscopy	22
Specimen Preparation	22
Test System and Test Condition	22
Fatigue Tests	23
Fatigue Test Equipment	23
Fabriction of Fabric Composite Fatigue Specimens	23
4. RESULTS AND DISCUSSION	26
Verification of Contact-Damage Fatigue Mechanism	26
Coating of Fibers	33
Effect of Graphite Content on the Fiber Surface	33
Establishment of Fatigue Test for Strand Composites	41
Effect of Silicon Rubber on Static Test	41
Effect of Silicon Rubber on Fatigue Test	42
Effect of Surface Treatment on Static Tensile Strengt	44
Effect of Coating on Strand Composite Interface Strength	46
Fatigue Resistance of Coated Fiber Strands.	47
Fatigue Resistance of Coated Fabrics	50

5. CONCLUSIONS AND RECOMMENDATIONS 55

REFERENCES 59

APPENDIX 64

LIST OF TABLES

Table Page

1. Comparison of Different Magnification Techniques 12
2. Mechanical Test Results of Fiber Strands 28
3. Element Analysis of Coated Fiber and Normal Fiber 35
4. The Effect of Silicone Rubber on Static Tensile Strength 41
5. The Effect of Coating on Strands Composite Static Strength 45
6. The Microdebonding Force for Different Fibers 46
7. Static Tensile Strength, So, of Coated, Control, and As-received Strands 47

LIST OF FIGURES

Figure Page

1. Damage Model During Fatigue Life 7
2. Fatigue Behavior of Different Composite Materials 10
3. Operation Sketch of AFM Detector 12
4. AFM Scanning Parameters 18
5. Microdebonding Apparatus..... 19
6. Micrograph of Polished Specimen Cross-Section 21
7. Instron 8511 Servohydraulic Test Machine 25
8. Tensile Specimen Geometry 24
9. The Geometry of Tab and Strand Composite Specimen 25
10. Large Range AFM Image of Fiber-Glass 27
11. SEM Image of Fiber-Glass 26
12. AFM Image of Fatigued Glass Fiber 29
13. Profile of Cracks 30
14. Effect of Probe Geometry 32
15. AFM Image of Sharp Crack 32
16. SEM Image of 1% Graphite Coated Fiber 34
17. SEM Image of 5% Graphite Coated Fiber 34
18. SEM Image of 3% Graphite Coated Fiber 35
19. Element Analysis Diagram for Coated Fiber 36

20. Element Analysis Diagram for Control Fiber 37

21. XPS Carbon Spectrum for Coated Fibers 39

22. XPS Carbon Spectrum for Treated Fibers 40

23. SEM Micrograph of Coated Fiber Surface After Transverse Tensile Test 41

24. Photograph of Broken Specimen 42

25. Fatigue Diagram of Specimens With Different Tab 43

26. SEM Micrograph of Debonded Fiber 46

27. S-N Curves for Glass Fiber Strand Composites 49

28. S-N Data for As-received Fabric Composite 52

29. S-N Data for of Control and Coated Composite Fabric composites..... 53

30. S-N Data for Different Batches of Fabric Composites 54

ABSTRACT

Glass fibers are the lowest cost and most widely used man-made reinforcement for composite materials . As a material for structural applications such as wind turbine blades, a major drawback is poor tensile fatigue resistance. This study has been concerned with identifying the cause of fatigue failures and with finding fiber coatings to improve the fatigue resistance.

As part of the study, a test method for determining the fatigue resistance of small strand composites was developed which allows rapid assessment of the effects of material parameters such as fiber coatings. The fatigue sensitivity obtained with this test was similar to literature values obtained at lower frequencies with larger specimens. The most important feature of the test method is a silicon rubber coated tab which reduces the problem of failures near the edge of the tab.

Previous studies of the glass fiber composite tensile fatigue mechanism have postulated that the poor fatigue resistance was due to fiber contact damage. In the current study, Atomic Force Microscopy has been used to analyze glass fiber surfaces. Fibers from composites subjected to fatigue were found to have scratches of significant depth in most cases; no such scratches were detected on fibers from static tensile tests. This result strongly supports the contact damage mechanism.

In an attempt to reduce fiber surface damage in fatigue, a graphite particle fiber coating procedure was developed. E-glass fiber composites with graphite particle coatings showed the same static strength but improved fatigue resistance relative to control samples. In the relationship S/So=1-b*Log N, where S is the maximum fatigue stress, So the static ultimate tensile strength, and N is the cycles to failure, the fatigue coefficient, b , for strand composites decreased from 0.10 for as-received fiber strand to 0.071 for coated strand. For fabric reinforced composites, the b value for as-received material was about 0.13 while that for the coated fabrics was about 0.089. In both cases, the coated fiber composite cycles to failure increased by about 100 times as compared with as- received fiber composites when S/So=0.5. Thus, the graphite particle coating was effective in increasing the fatigue resistance without reducing the ultimate tensile strength. The fiber/matrix bond strength was also unaffected, so that material properties dominated by the matrix/interface should not be changed significantly.

CHAPTER ONE

INTRODUCTION

When the application of a material to an engineering component is contemplated, it is essential for the material to be not only physically and mechanically satisfactory for the service requirement, but also competitive in cost. This is nowhere more evident than in the newly resurgent wind energy industry, where glass fiber composite is considered to be more appropriate than carbon fiber composite because of its lower cost. The wind turbines are designed to be inexpensive, light weight, efficient, and produce electricity for communities at a rate competitive with current gas and possibly coal facilities. To achieve these objectives, manufacturers use E-glass/ polyester or vinyl ester composites for their turbine blades.

Glass fibers are the cheapest and most widely used man-made composite reinforcements. As structural materials, their major limitation is lower modulus-to-density ratio as compared to carbon fibers [1] . As a potential material for a turbine blade, however, another major drawback is the poor tensile fatigue resistance of glass fiber composites [2].

The poor tensile fatigue resistance of E-glass composites has been shown by Mandell, et. al, to be a basic fiber dominated property [3]. The cyclic tensile fatigue produces a stress versus log cycles to failure (S-N) fatigue lifetime trend of about 10 percent of the one cycle strength per decade of cycles. It was proposed by Mandell, et. al, that the basic mechanism of fatigue appears to be contact damage between fibers [3]. A number of attempts have been made to overcome this problem, but none of them has been commercially successful [4].

The present study extends earlier work in exploring the tensile fatigue mechanism and

finding a commercially viable method for improving the fatigue resistance. The present study also covers the development of a fatigue resistance test method for small material samples.

CHAPTER TWO

BACKGROUND

General Fatigue Properties

The long-term behavior of composite materials has been the subject of active research in recent years [5]. It appears that the fatigue behavior of a fiber composite differs in fundamental ways from that of a metal or unreinforced polymer. The term "fatigue" refers to the repeated cyclic mechanical loading of a material; in this discussion, the force versus time relationship is usually sinusoidal , with the mean force and amplitude controlled to be constant throughout the experiment, until failure occurs.

Fatigue Behavior of Metals

Metals are polycrystalline aggregates. During stress cycling, microdamage develops in the form of microcracks, void growth, and plasticity within single crystals. The fatigue process is generally characterized by three stages: initiation, propagation, and final fracture [6]. In metals, crack initiation is caused by localized plastic deformation resulting from dislocation motion. Initiation can consume a large portion of the lifetime. After initiation, stage I growth occurs when a single crack forms and propagates along the same crystallographic plane where slip had taken place. Stage II growth occurs when the crack can propagate normal to the tensile stress, regardless of the crystallographic plane. Stable crack growth can be described as a repeated crack tip blunting process [7]. Plastic flow at the crack tip initially blunts the crack, reducing the stress concentration . As cycling continuous, the

amount of plastic flow is decreased as the metal is work hardened. After some time, the material at the crack tip can no longer blunt the crack and the crack advances. Eventually, final fracture occurs when the crack is sufficiently long to become unstable at the maximum load [8].

Fatigue Behavior of Polymers

In unreinforced polymers, there are three modes of fatigue failure: creep deformation, thermal melting, and crack propagation [9]. Creep deformation is not strictly considered a fatigue process since it can be viewed as elongation induced by a sustained loading pattern. Essentially, since polymers can fail under a steady applied load, they can also fail by the same cumulative mechanism under interrupted loading.

The second mode of failure is thermal failure. This mode can operate depending on the amount of hysteretic energy generated during each loading cycle [10]. As this energy is dissipated as heat, an associated temperature increase will occur. The temperature can rise to a sufficiently high level to melt the sample. Thus, failure occurs by viscous flow. On this basis, fatigue life increases with decreasing frequency of loading. Another parameter involved with thermal failure is the heat transfer characteristics of the specimen. Since better heat conductance should lead to longer fatigue life, a greater surface area to volume ratio increases lifetime. Even if these qualities are designed into a part, fatigue failure by a mechanical mode is still possible.

The third mode of fatigue failure is the initiation and propagation of cracks [11]. In glassy thermoplastic polymers and some semicrystalline polymers, the cracks are preceded by craze formation. The craze formation is analogous to the formation of a plastic zone in

metals in that it effectively blunts the crack and absorbs energy. The long, thin fibrillar craze grows continuously during the cycling process. However, its growth rate is slower as the craze length increases. When the craze reaches a critical condition, the crack advances abruptly through the craze and then stops. With continued cycling, a new craze is developed and the process continues. This propagation process leads to a growth band surface morphology in which many cycles are required to form one band. At higher stress intensity levels, the formation and breakdown of the craze material can occur during one cycle, leaving striations on the fracture surface. The striations mark the position of the crack front for each cycle. In crystalline polymers that do not craze, there are different energy dissipation mechanisms. Energy is absorbed when the crystallites deform due to the applied stresses. The possibility also exists for the deformed sections to reform into a different, possibly stronger crystalline structure. Fatigue behavior is shown to be improved with increasing crystallinity, increasing molecular weight, increasing volume of crazed material, and the presence of low temperature dissipation processes.

More brittle thermoset polymers, such as those used in this study, do not generally form crazes [12]. The fatigue process is by the initiation and advance of a brittle crack. The detailed crack tip mechanisms have not been clearly identified for these polymers. Like most brittle materials, thermoset polymer have a relatively high fatigue crack growth exponent (Slope of a log-log plot of crack growth rate versus stress intensity factor) [6].

Fatigue Behavior of Fiber Composites

The fatigue behavior of fiber composites varies greatly compared with that of homogeneous materials. This is due primarily to the high degree of heterogeneity and anisotropy in composites [13].

Fatigue damage in metals and polymers is usually the result of a single crack that propagates into the body of a component. As such, the decrease in residual strength and fatigue crack growth can be modeled using fracture mechanics. In contrast, the fatigue damage in reinforced plastics is usually progressive and extends throughout the stressed area of the specimen [14]. Many microcracks can be initiated on the first cycle if the stress is sufficiently high. In these cases, much of the life-time can be spent in combining the microcracks into macrocracks, reducing the residual (remaining) strength of the specimen. Final separation will occur when the residual strength equals the maximum stress of the load cycle. Although the specimen is cracked, prior to final fracture, primarily in the matrix and interface areas, the component may still be sufficiently strong to be acceptable in certain applications . However, the cracking, which can affect properties such as the apparent elastic modulus, Poisson's ratio, and solvent resistance, may make the composite unsuitable for other applications [15]. Eventual failure usually corresponds to a significant density of fiber failures.

The critical elements identified for fiber reinforced polymers are fiber tensile failure, matrix cracking, interlaminar debonding crack growth, and local compressive instability. These failure modes appear in different stages of the fatigue damage development. Recent work by Reifsnider [12] has shown that the fatigue life can be separated into four stages for

a typical multidirectional laminate. In Stage I, matrix and interface cracking develops in layers with fibers at some angle to the maximum stress dominate. This stage occupies the first 10-15% of fatigue life. The number of cracks reaches a saturation, CDS (Characteristic Damage State), state at the end of Stage I while fiber fractures are rare. In Stage II, matrix/interface cracks coalesce at intersections in adjacent layers through interlaminar separation between layers. In Stage III, delaminations spread to separate the plies over much of the specimen area. Finally, in Stage 4, fibers failures in the 0° plies (Plies with fiber in the load direction) accumulate until the 0° , load bearing plies fail, representing total specimen failure (Figure1).

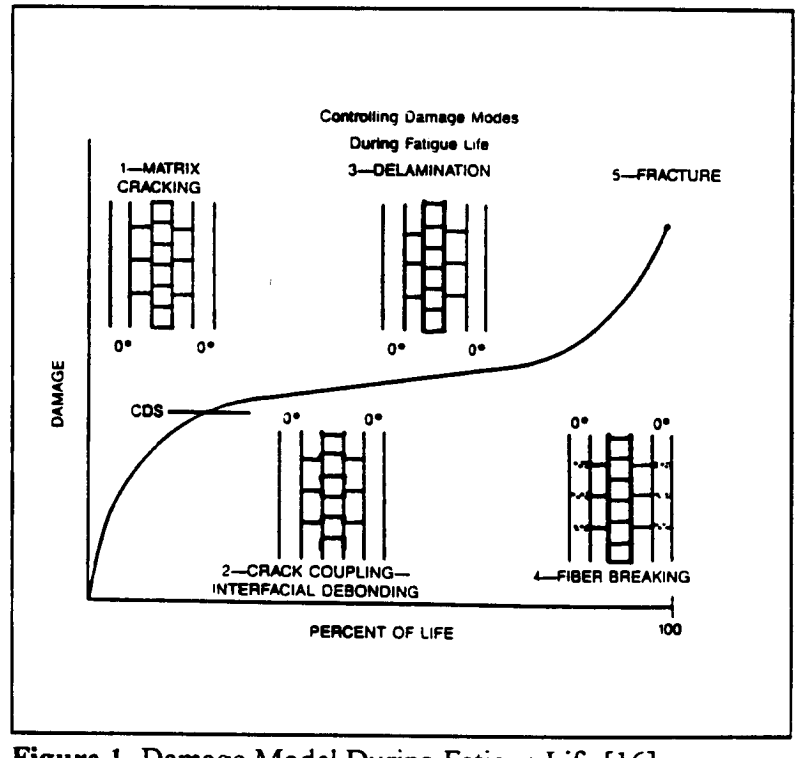

Figure 1. Damage Model During Fatigue Life [16]

As discussed above, the fatigue behavior of composites is more complex than that of homogeneous materials. The general features described by Mandell [17] are as follows:

1. Failure is usually progressive, resulting from the gradual accumulation and interaction of dispersed damage, rather than by the nucleation and growth of a dominant crack.

2. As damage accumulates, the constitutive relations of the material may change significantly.

3. A number of distinct damage modes can be identified, including fiber-dominated tension and compression, matrix-dominated cracking parallel to the fibers, and interlaminar cracking between plies. Some of these may produce failure directly while others may have an indirect effect on failure by causing load transfer onto the fibers.
4. Under tensile loading the strains to produce matrix cracking are generally well below those to produce fiber failure. As a consequence, in multidirectional composites, cracking tends to initiate first in domains (plies) where the fibers are at the greatest orientation relative to the maximum tensile stress. Cracking then accumulates in these domains, followed by domains or lesser orientation.
5. Large-scale delamination between plies has been a significant failure mode for composite structures, particularly with out-of -plane loads.

Although these features are common to a broad range of fiber and matrix systems, the actual fatigue behavior depends strongly on the type of fibers and style of reinforcement [18].

Fatigue Behavior of Glass Fiber Reinforced Composites

For glass fiber-reinforced plastics (GFRP), there exits two different kinds of fatigue phenomena, static fatigue and cyclic fatigue [19].

Static fatigue results from stress corrosion of the fibers. Under the combined influence of a stress and a corrosive environment, GFRP may fail at much lower stresses than in the absence of the environment.

Static fatigue of fibers is generally assumed to be due to crack growth within individual fibers caused by the stress-activated silica-water reaction [20]. Metcalfe, et. al, [21] have

shown that spontaneous cracking of glass fibers occurs in acids even in the absence of an externally applied stress. They attribute this to an ion exchange process in which the metal ions in the glass are replaced by hydrogen ions from the acid. The subsequent shrinkage of the outer layer of the fiber results in surface tensile stresses which lead to failure. Alternative explanations of spontaneous cracking based on leaching of the material at the tip of pre-existing flaws and exchanges in the surface tension at crack surfaces have been proposed by Weiderhorn [22]. However, later work suggests that high-strength fibers have a flaw-free surface and so the weakening may be due to flaw initiation rather than crack growth [23]. Recent work has also found that the matrix toughness has some effect on the fatigue behavior [24]. In GFRP with a less-tough resin, cracks which allow an acid penetration are easily produced. The higher the toughness, the more difficult is the crack formation, and this leads to the maximum strength in low strain-rate tensile tests at some optimum matrix toughness range. Above this range, limited yielding becomes noticeable, which restricts the growth of cracks, resulting in greater retention of original strength. However, this lessens the original strength value itself. Therefore, there is an optimum value of matrix toughness giving the maximum resistance to static fatigue.

The static fatigue behavior of glass fibers is consistent with that of bulk glass [25], but cyclic loading effects are not present in bulk glass or individual fibers. Cyclic fatigue effects are seen only in multi-fiber arrangement.

Earlier work by Mandell and coworkers [26] has shown that the E-glass composite longitudinal cyclic tensile fatigue resistance is the poorest among all composites. The variation of fatigue resistance for different composites is illustrated in Figure 2 [27].

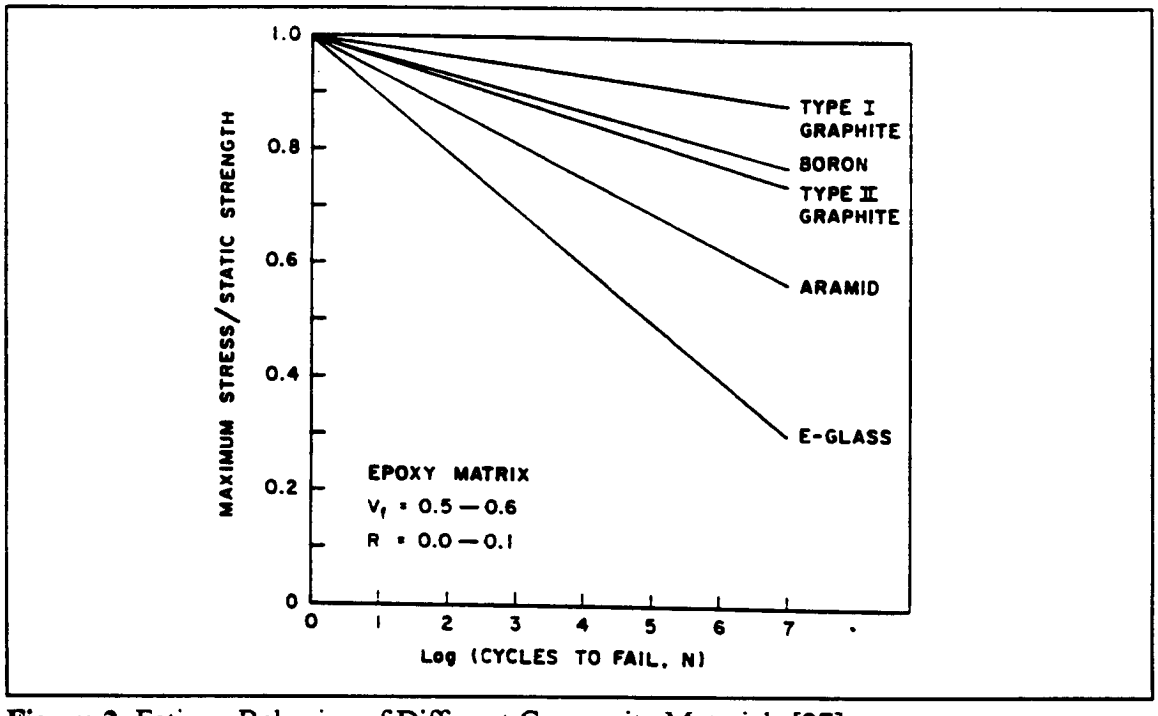

Figure 2 Fatigue Behavior of Different Composite Materials [27]

It was found that the Type I, high modulus graphite composite is almost completely insensitive to fatigue while the E-glass composite will lose approximate 10% of the initial static strength per decade at typical tensile fatigue loadings conditions, such as R=0.1(R is the ratio of minimum to maximum stress on each cycle).

This poor tensile fatigue resistance is attributed to fiber interaction by Mandell et, al. [3], They found that strands of as few as 30 fibers still show the characteristic stress-cycle lifetime trend of larger volumes of typical test specimens and this behavior doesn't depend on the type of matrix and bonding [28]. Single fibers are not sensitive to cyclic stressing. Composites made from specially fabricated large diameter glass fibers with residual compressive stresses on the surface have even better fatigue resistance than that of carbon fiber composites [29]. Based on the above observations, Mandell et. al postulated that the basic mechanism appears

to be local contact, fretting-type damage at points where fibers contact each other along their length.

This mechanism has been challenged by the fact that there is no damage on the surfaces of glass fibers subjected to fatigue has been documented to date [30] . One explanation to this is that the cracks are closed [31]. Another explanation suggests that the strength-impairing flaws may be subsurface [32]. Besides the above explanations, stress corrosion was also used to explain this poor fatigue resistance. Dharan [33] perceived that stress corrosion cracking of glass fibers at the tip of a matrix crack controlled the cracked growth rate. However, he did not establish the validity of this suggestion [34].

It seems that the key point for Mandell's explanation is weather the lack of observation of fiber surface damage is due to the lack of surface cracks or due to the difficulty of observation.

Analysis of Composite Interfaces

Imaging of Fiber Surface

Many techniques are available for magnifying the detailed features of a surface. Methods for magnifying surface features originated with magnifying lenses and optical microscopy in the late 18th century. During the 20th century, methods for magnification based on electron and ion beams have been developed . Table 1 compares magnification techniques with regard to magnification, operating environment, type of image and damage to the sample [35].

Table 1. Comparison of Different Magnification Techniques

Technics	Mag. Factor	Medium	Image	Damage
Optical	10^3	Air, Liquid	2-D	None
Laser Scan	10^4	Air	2-D	Minimal
Ion Beam	10^5	Vacuum	2-D	Severe
SEM	10^6	Vacuum	2-D	Some
AFM	10^9	Liquid, Vaccum, Air	3-D	Minimal to None

Among these techniques, the scanning electron microscope (SEM) is most widely used in research on composite materials [36]. However, SEM, which operates only in vacuum and requires a conductive coating, can only characterize fiber surface morphology down to the fraction of a micron scale [37]. A typical glass fiber has a diameter of 10 um, and possible surface cracks should be on the scale of nanometers. Therefore, the SEM is not capable of detecting fatigue damage on fibers.

The Atomic Force Microscope (AFM) was developed in the early 90's. As shown in Figure 3, the force sensor measures the deflection of a cantilever. An atomically sharp tip is mounted on the cantilever such that, when the cantilever moves, the light beam from a small laser moves across the face of a four section photo.The

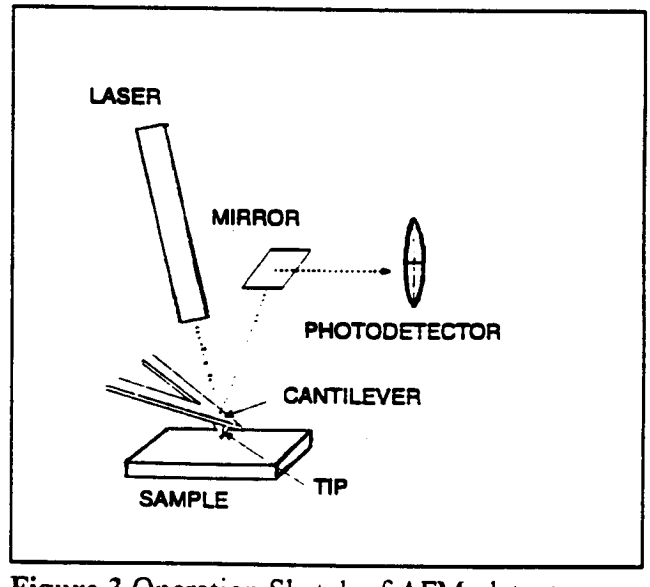

Figure 3 Operation Sketch of AFM detector.

amount of motion of the cantilever can then be calculated from the difference in light intensity on the sectors. Hookes law gives the relationship between the cantilever motion, X, and the force required to generate the motion, F , F=-KX.

It is possible to fabricate a cantilever with a force constant, K, of 1 newton/meter [38]. Since motion of less than 1 angstrom can be measured, forces less than 0.1 nanonewton are detectable. Therefore, AFM can image surfaces with a resolution of Angstroms. With the advent of first commercial AFM in 1990, this technique has been used to study the surfaces of a variety of materials, including ceramics, diamond films, liquid crystals, polymers, graphite intercalation compounds, DNA, etc. The first AFM study of carbon fiber surfaces was published in 1992 [39]. However, to our knowledge, there has been no report to date on AFM study of glass fibers used in composites .

If an appropriate AFM scanning method for glass fiber surfaces can be established, it should be able to detect some cracks (or scratches) on the fiber surface. If some surface cracks can be detected in the specimen having been run in fatigue test while there is no such cracks are detected on the surface of control fibers, the contact damage mechanism will have been verified.

If the poor fatigue resistance of GFRP is due to contact damage, it could be improved by decreasing the contact damage. An appropriate surface treatment method might be used to achieve such a purpose.

The Effect and Characterization of Composite Interface Strength

1) The Effect of Interface Strength on Composites

The interfacial bond between the matrix and the fibers is an important factor influencing

the mechanical properties and performance of composites [40]. The interface is responsible for transmitting the load from the matrix to the fibers, which contribute the greater portion of the composite strength. Strong adhesion between fiber and matrix favors most mechanical properties of composites such as compressive strength and transverse tensile strength [41]. However, there is at least one composite property, namely, the fracture toughness for through-thickness notches, which may be improved by decreasing adhesion [42]. The interface also has some effect on composite fatigue behavior. Hofer et al. [43] studied the fatigue behavior of glass-fabric composite having four different finishes, including an untreated surface and surface treated with Volan A, A-1100, and S-550 finishes (organosilane coupling agents.) The untreated glass exhibited the highest fatigue strength in a dry environment, but it was also the most severely affected in a humid environment. As a result, all fabrics showed a similar resistance to fatigue when tested in a humid environment. Although it has not been possible to predict the exact interface strength required for a particular system, it is clear that there exists a corresponding optimum bonding strength for any particular system to get maximum utilization of fiber properties. In order to keep other interface related properties (except fatigue resistance) unchanged, it is necessary to keep the interfacial strength approximately constant. Therefore, the interface strength of glass fiber/ resin matrix composites should be monitored by an appropriate test method when the fiber surface condition is altered.

2)Characterization of Interface Strength

There are several methods for testing interface strength, including the fiber pullout test

[44], wet work test [45], shear strength test [46], Raman spectroscopy [47], and micro-debonding test [48]. All of these tests, except for the micro-debonding test are based on model systems, in which the components of the system do not have the same arrangement or processing history as that found in actual composite materials [49]. Model systems can only correspond in a limited way to actual composite materials. Results from such tests can yield relative information about interfacial strength of various systems, but are limited in their ability to yield quantitative values of interfacial bond strength applicable to actual composite materials. The Micro-debonding test, however, can determine the interfacial strength of actual composite materials. It measures the bond strength by directly compressively loading individual fiber ends on polished cross-sections, with the maximum interfacial shear stress at debonding calculated through a finite-element based micromechanics data reduction scheme.

Characterization of Fatigue Strength

Another related technology requiring development is a test method to measure the fatigue resistance of small composite specimens at a high frequency. Although some high frequency fatigue test methods have been successfully developed in MSU [50], they can only be used to test laminate specimens. The high frequency is a convenience for rapid evaluation. In the present study, some candidate coating methods, such as plasma coating, can only treat small fiber strands. Therefore, the existing test method cannot be used directly. Small strand tests have been reported in low frequency tests in Reference 3, and a test of this type is developed in this study.

CHAPTER THREE

EXPERIMENTAL METHODS

Coating of Strands and Fabrics

Graphic flake coating mixture

In the coating method used here, 8 g of epixode (Buchler, No. 20-8130-032) was added into 100g general purpose absolute alcohol. A magnetic stirrer was used to stir the mixture until the epixode was completely dissolved into the alcohol. A silane Coupling Agent (1 g, Dow Corning, Z-6032) was then added into the solution, and 20g of Conductive Carbon Paint (SPI Supplies, SPI# 5006) with 20% by weight of graphite flakes in alcohol was slowly dropped into the epixode/coupling agent/alcohol solution. The mixture was then immediately used to coat the fibers.

Fiber Coating

1) Strand Coating.

Five-inch-long E-Glass Strands (Owens Corning, 102A-AA-56 Fiberglas^{R} Brand Multi-End Roving) were bonded at both ends with super-glue. The strand was immersed into the coating mixture for about 15 seconds and then picked up by holding one end. A soft towel was used to wrap and sweep the strands in order to keep the strand well aligned and to absorb extra mixture. Fiber content was not controlled because the strand was not cured in a mold (fiber volume fraction may be significant if it varied in a wide range). The coated strands were hung over night at room temperature and then kept in a clean box for further use.

2) Fabric Coating.

Two layers of Hexcel D155-Y unidirectional E-glass cloth were put into an RTM (Resin transfer molding) mold following the same procedure used to make fatigue specimens described below. The coating mixture was injected into the mold. The mixture was held in the mold for 5 minutes. The injector tube was then released to let extra mixture run out. Compressed air was connected to the mold to dry the fabric overnight. The fabric thus treated was used to make fatigue specimens by RTM.

Atomic Force Microscopy

Specimen Design

Single fibers were taken from the fracture section of preciously fatigue or static tested specimens. Xerox conductive graphite powder (10% by weight) was added into epixode to obtain a conductive adhesive mixture, which was then put into a casting cup . Fibers were carefully put on the surface of the mixture immediately after it had reached the gel point. The specimen was kept in a desiccator overnight. These fibers, which were partially but firmly bonded to the resin matrix were used for AFM scanning. An alternative preparation method using the Micro-debonding apparatus, provided better specimens. The same mixture was used but the fiber was not attached onto the mixture surface until it had reached a rubbery state. The fiber was pushed into the mixture with the microdebonding apparatus, using a flat ended probe.

Test Apparatus

The AFM apparatus used here was a TMX 2000 Discoverer Scanning Probe

Microscope made by TopoMetrix. The TMX 2000 consists of following sub-systems: computer(CPU), electronic control unit(ECU), microscope stage, and video monitor. ECU provides the electronic signals that control the scanner, positioning devices, and amplifiers in the microscope stage and chassis. The standard *Discoverer* stage has integrated vibration isolation, an optical microscope and a computer-controlled Sample Positioner. A S92713AL scanner with maximum scanning range of 1 um and a S925B20CL scanner with maximum scanning range of 25 um were used.

Test Procedure

Samples were mounted onto a stainless steel holder which is magnetically held to the piezoelectric scanner. The holder is grounded by a wire. After the sample was mounted, the cantilever was set in the holder. For accurate measurements the cantilever must be seated firmly in the holder. The AFM required alignment before scanning the sample. The alignment included aligning the Laser Head and aligning the Laser Head assembly and optical microscope. The scanning control parameter was set using the computer. A set of typical control parameters is shown in Figure 4.

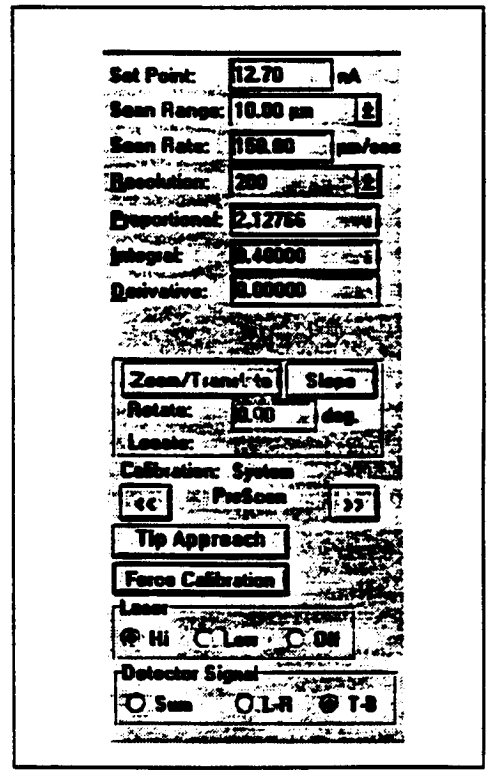

Figure 4. AFM Scanning Parameters

Microdebonding Test

The microdebonding testing system used in this study is a modified version of the one originally developed by Mandell, et al at MIT [48]. The overall test system consisted of two major assembly stations as shown in Figure 5. They are the microscope and microindentation station and the auxiliary monitor and printer station. The microscope and microindentation station are mounted on a vibration isolation platform (Kinetic Systems, Model 2212) to reduce the effects of floor vibration. The research quality optical microscope (Leitz Wetzlar,

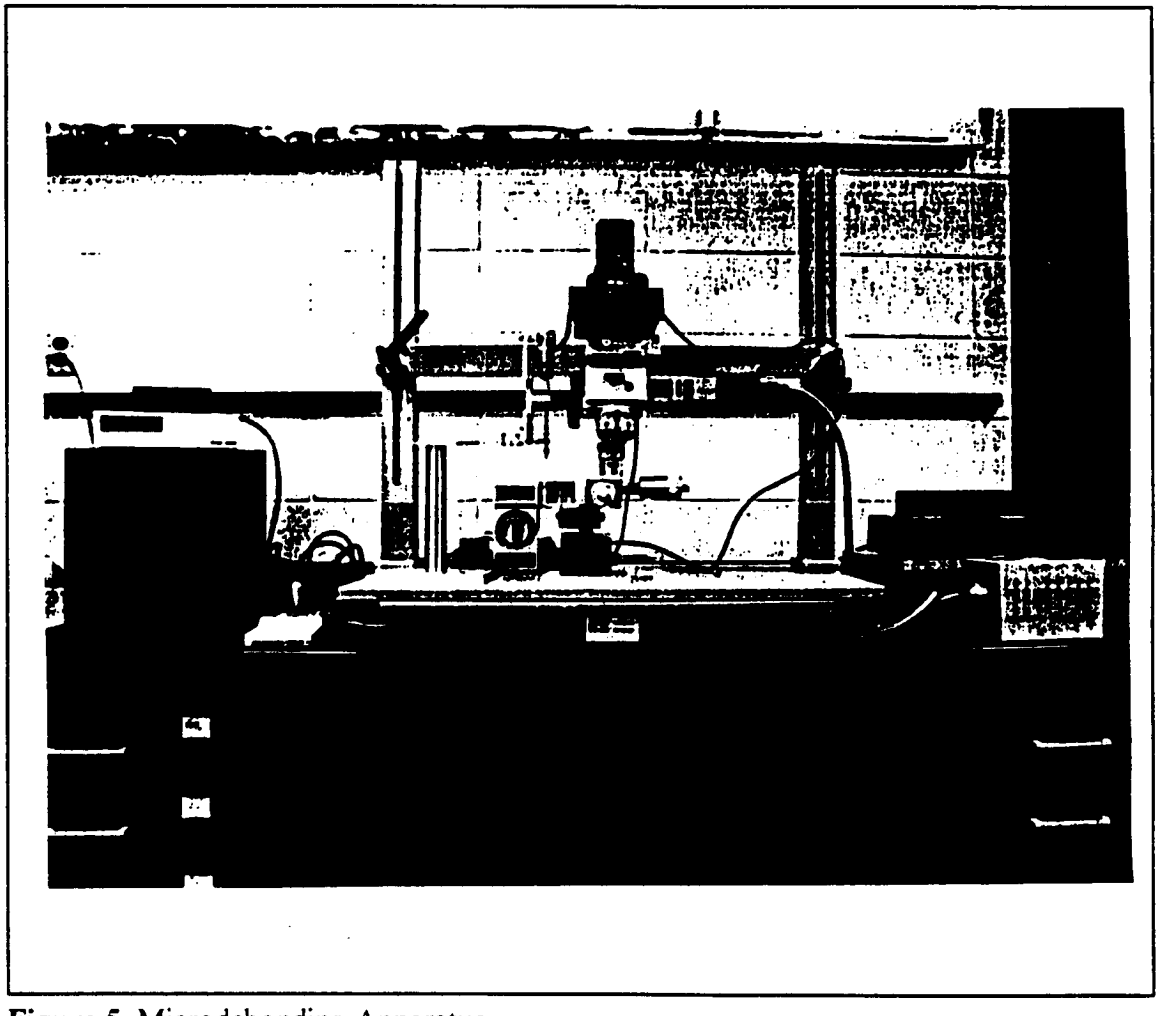

Figure 5. Microdebonding Apparatus

Model 563 483) has a video camera attached on the top, and uses 100, 50, and 10X objectives and a 2X eyepiece that bring a maximum of about 2000X magnification.

The translation stage subassembly is below the microscope objectives. It consists of an XY axis micrometer drive stage (Newport, Model M-462-XY) with 0.1 um accuracy for location of the specimen relative to the probe position, a rotary stage (Newport, model M-481) with magnetic stops for reproducible movement of specimen between the probe location and optical axis of the microscope with an accuracy better than 1 um, and a vertical translation stage (Newport, Model M-416) for raising the specimen positioned under the probe for load application. A force transducer (Schaevitz, Model FTD-G-100) with 1 mN resolution is used in this apparatus.

Specimen Preparation

Specimens for the microdebonding test consisted of composite laminate or strand composites which had been sectioned perpendicular to the reinforcing fibers. Specimens were then potted in an epoxy compound in plastic casting cups. Plastic specimen support clips were used to insure that the specimens were positioned perpendicular to the bottom face of the casting cup.

Grinding and polishing of the mounted specimen were performed on a Buehler, metallographic polishing bench. The specimens were first roughly polished with a series of silicon carbide grinding papers, from 120 grit to 800 grit, and then finely polished with grinding papers from 1000 grit to 4000 grit. The specimen cross-section was microscopically examined between each step. Polishing was continued until virtually no scratches were visible

on the surface of the specimen when observed at the magnification used for testing. Sometimes the specimen was polished with a silk cloth mounted on the polishing wheel. A diamond slurry (15 um to 1/4 um) was dropped into cloth while polishing. An example of the polished surface is shown in Figure 6.

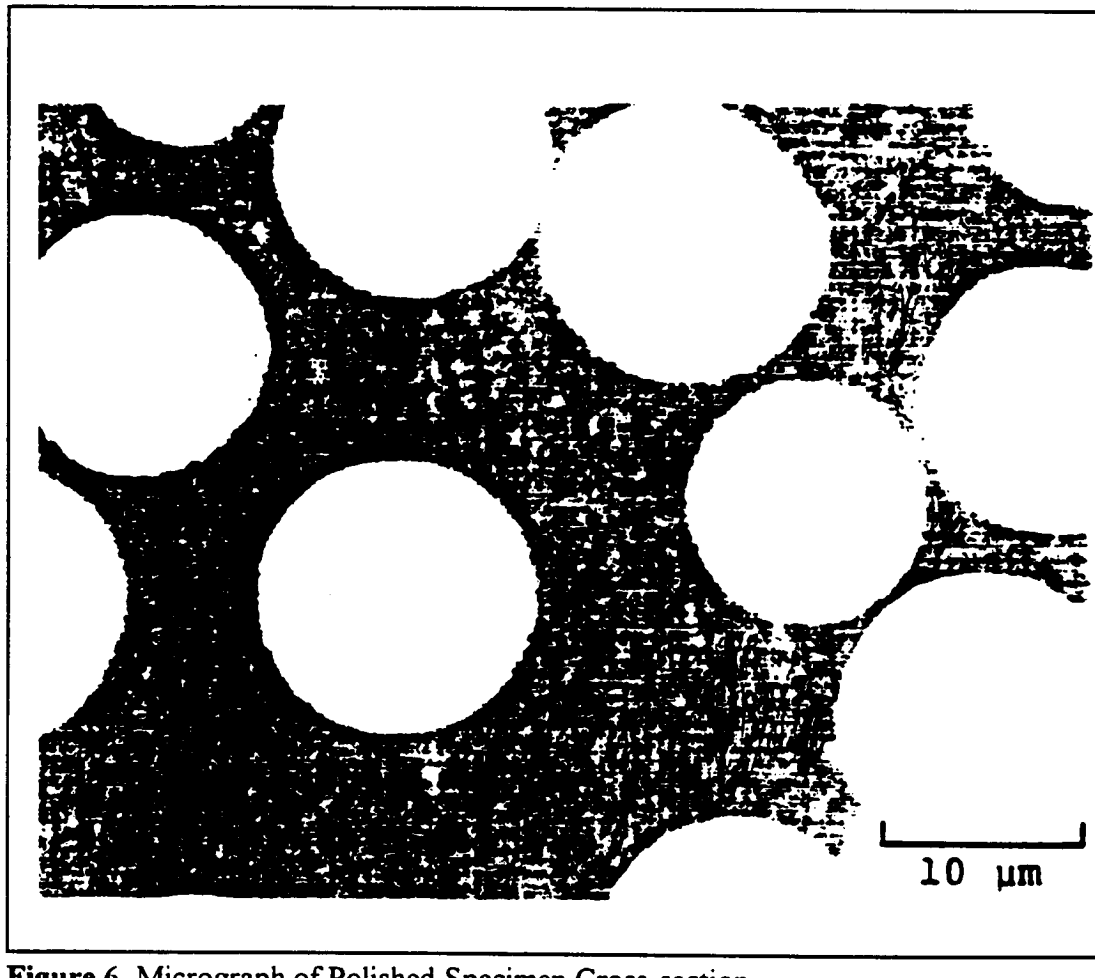

Figure 6. Micrograph of Polished Specimen Cross-section

Test Procedure

After a specimen is mounted on the stage, calibration of the load transducer and alignment of probe are carried out before testing. The calibration of the load transducer is

checked using analytical weights. A working curve of load versus output current is made. The alignment is done through a sequence of adjusting the probe position and viewing the location of the mark made by probe. This procedure continues until the mark always appears in the center of screen of the video monitor.

The test begins by locating the region of interest on the specimen using the XY translation stage. The center of the fiber of interest is moved to the marked point on the monitor representing the loading point of the probe. The specimen is then raised slowly using the vertical translation stage until the probe contacts the specimen and the desired load is indicated. After holding the load for about 5 seconds, the specimen is unloaded by lowering. The rotary stage is then rotated back to the optical axis of the microscope. The specimen is inspected for initiation of debonding or evidence of off-centered loading or probe sliding. The fiber end is incrementally loaded and observed under the microscope between each loading step until debonding is detected.

Scanning Electron Microscopy

Specimen Preparation

The samples for SEM analysis were first mounted with conductive tape onto sample holder. The samples were first sputter-coated with gold/palladium to eliminate surface charging effects. The thickness of the gold layer was about 25 nm. The coated samples were stored in a desiccator for further use.

Test System and Test Condition

The SEM used in this study was a JSM-6100 electron microscope located in the ICAL

Laboratory in the Department of Physics at Montana State University.

The electron gun source is LaB_6 and the scanning current is 3.0 A. Pressure is 10^{-7} torr in the analysis chamber. Element analysis was carried out by Energy Dispersive Spectroscopy (EDS) in this SEM system in the EDS mode with the same conditions as in the SEM mode. The EDS detects elements by study of emitted X-rays from the sample. The electron beam is introduced to the sample to produce characteristic X-rays.

Fatigue Tests

Fatigue Test Equipment

A high response, low force Instron Model 8511 servo hydraulic test machine was used for static and fatigue testing (Figure 7). It has a 15 gallon per minute (GPM) servo valve and operates at 3000 psi hydraulic pressure supplied by a 20 gpm pump. A 2248 lb. load cell and a 500 lb. load cell were used for fabric and strand composites respectively.

All tests were conducted under load control. The loading rate for static test were determined by the frequency under which fatigue tests would be run. Fatigue tests were run with constant force amplitude sine waves. The amplitude and average load were determined from the R value (ratio of minimum to maximum load) and maximum stress level of each test. Experiments were conducted in ambient air with temperatures ranging from 65 to 80 degrees Fahrenheit and low humidity (10-14% R.H.).

Fabrication of Fabric Composite Fatigue Specimens

The fabric composite specimens were fabricated from Hexcel D155-50 unidirectional E-glass cloth by RTM. Procedures followed those developed by Belinky [50] except that

the specially coated fabric cloth was used in this study. The specimen geometry is shown in Figure 8.

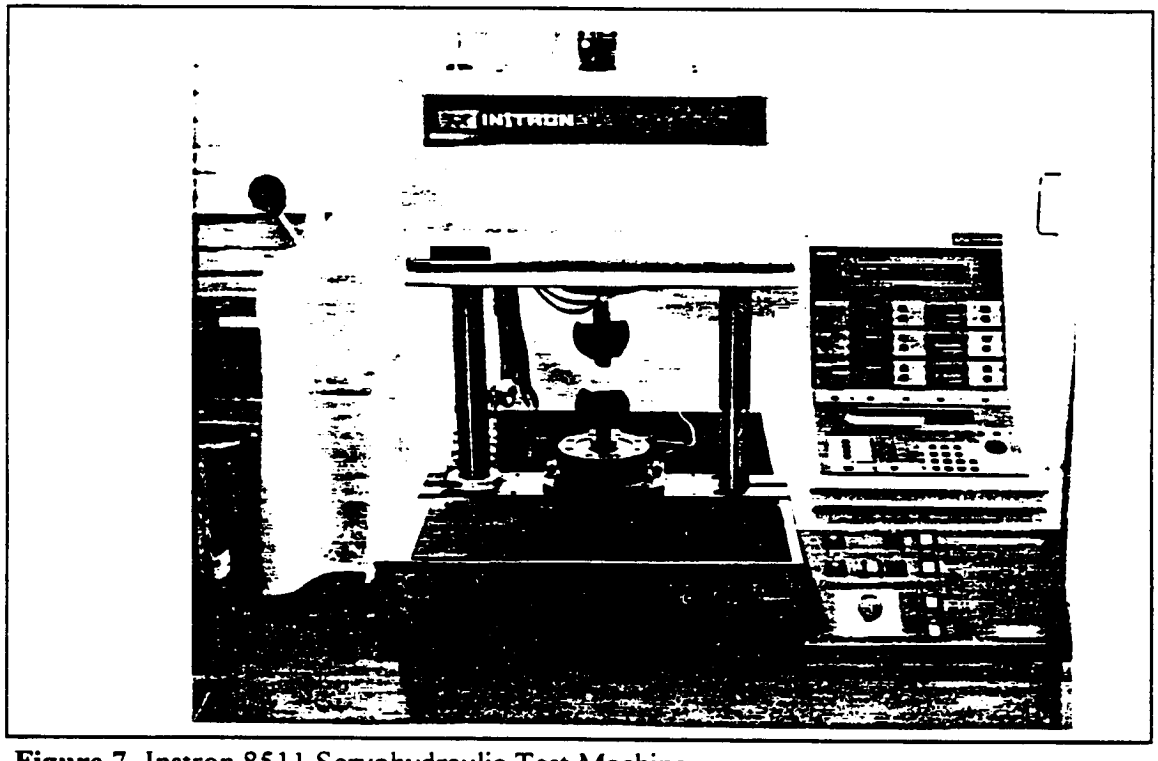

Figure 7. Instron 8511 Servohydraulic Test Machine

The coated strands were impregnated with the polyester resin by drawing them through a resin bath, clipping them to a frame under a slight tension, and finally curing them at ambient temperature. The impregnated strands were attached to cardboard tabs for testing. The strands were bonded with two adhesives. An epoxy (Hysol Engineering Adhesives, EA 9412, Dexter Aerospace Materials Division) was used to bond the strands to the middle of the tabs and a silicone rubber adhesive (RTV 735 Sealant, Dow Corning) was used to bond the strands at the end adjacent to the gage section. The tabbed specimens were heated for two hours at 120 °F to cure the epoxy. The length of the gage section is 2.54 mm. The geometry of the tab and strand composite specimens are shown in Figure 9.

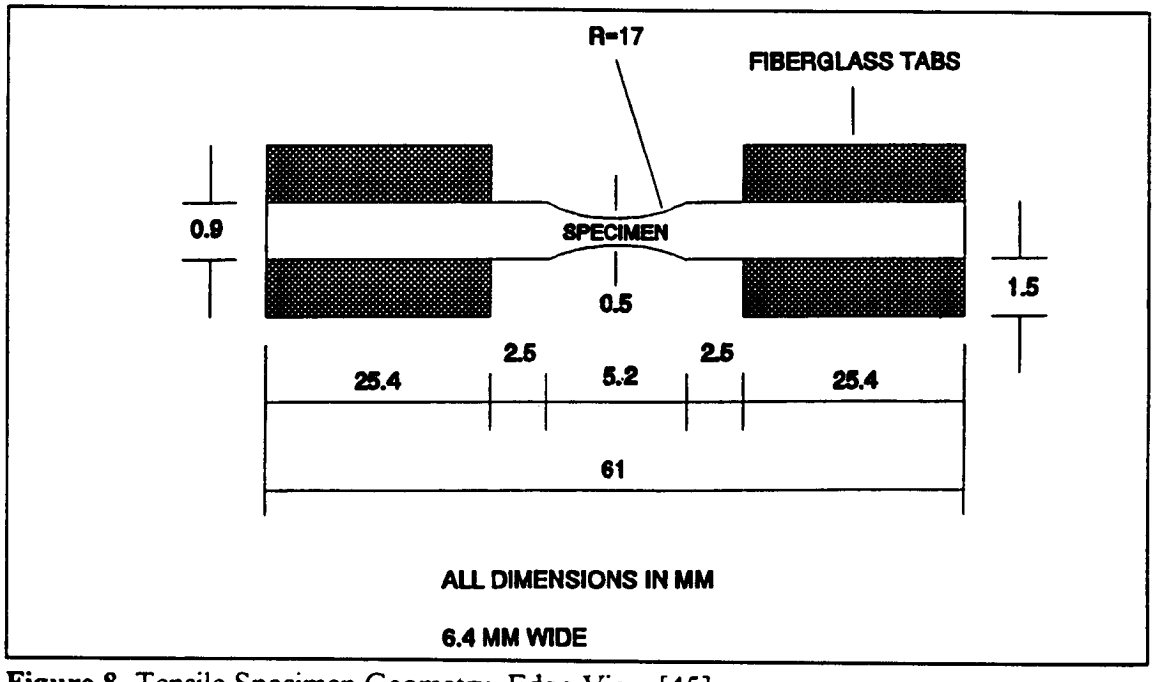

Figure 8. Tensile Specimen Geometry, Edge View [45]

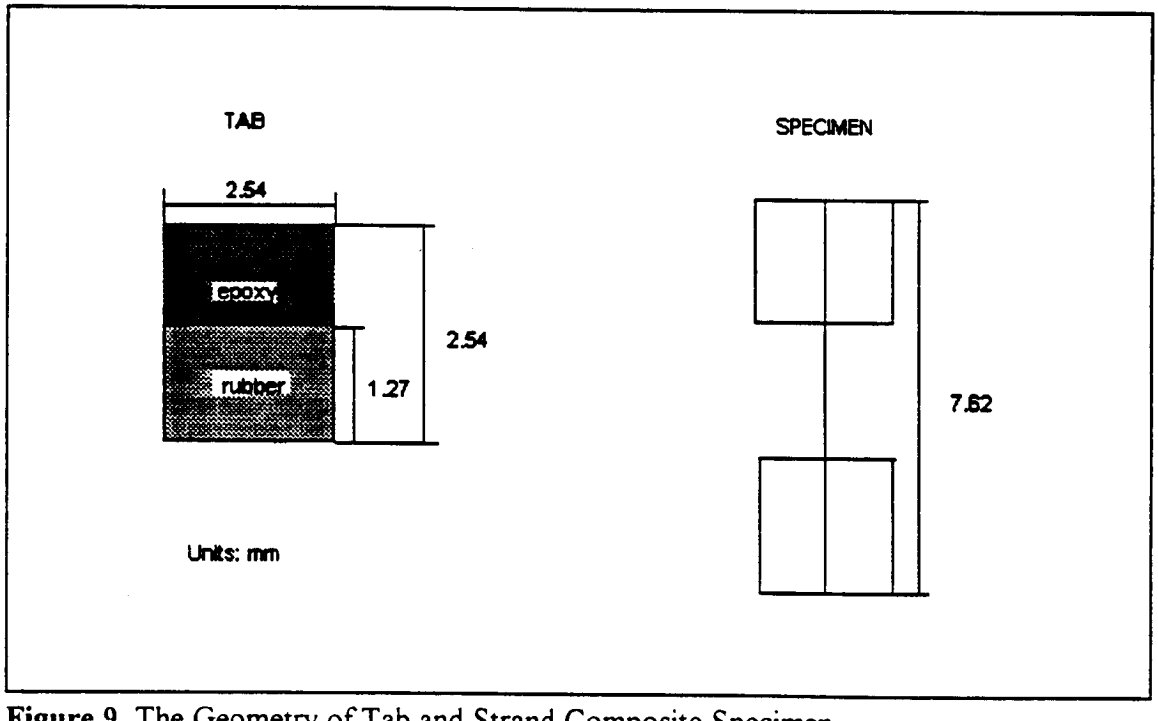

Figure 9. The Geometry of Tab and Strand Composite Specimen

CHAPTER FOUR

RESULTS AND DISCUSSION

Verification of Contact-Damage Fatigue Mechanism

Fibers were taken from both static broken tensile specimens and fatigued specimens. These fibers were then used to prepare AFM scanning samples by the methods described in Chapter 3.

The fibers were first scanned with the large scanner (Tip), S92713AL, which has a scan range of 10 um. Scanning with this scanner can give a low magnification image of the fiber. A typical image of the fiber is shown in Figure 10.

From this figure, it is found that the large range image of the fiber is the same as that usually observed with SEM (Figure 11), which means that the AFM runs well.

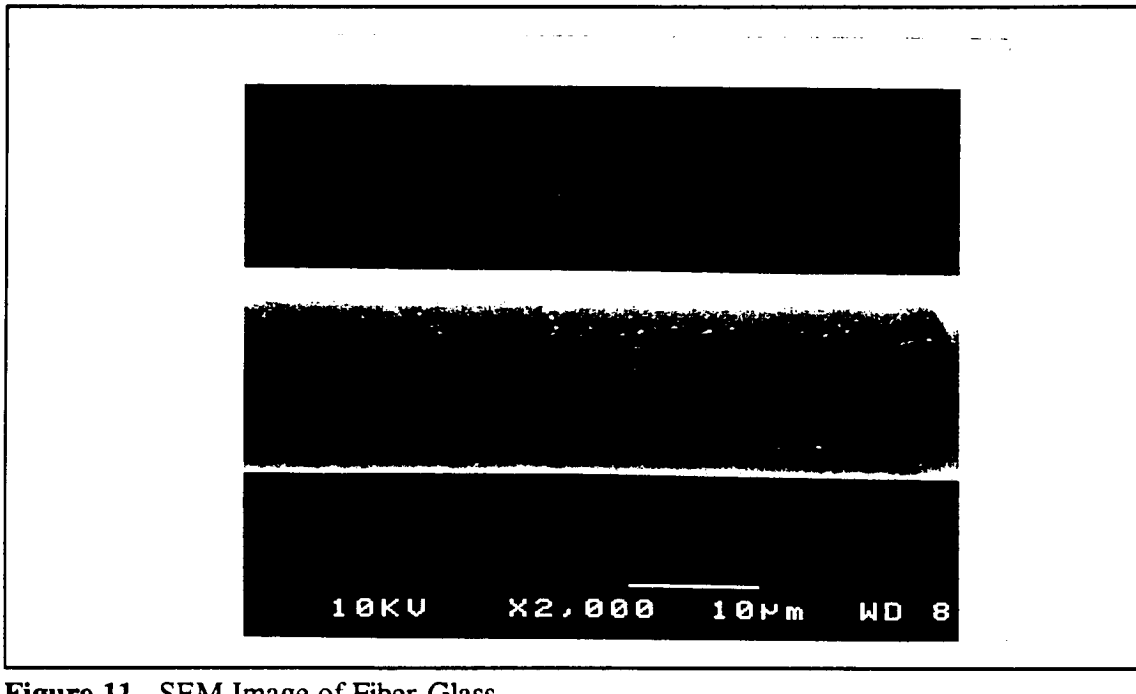

Figure 11. SEM Image of Fiber-Glass

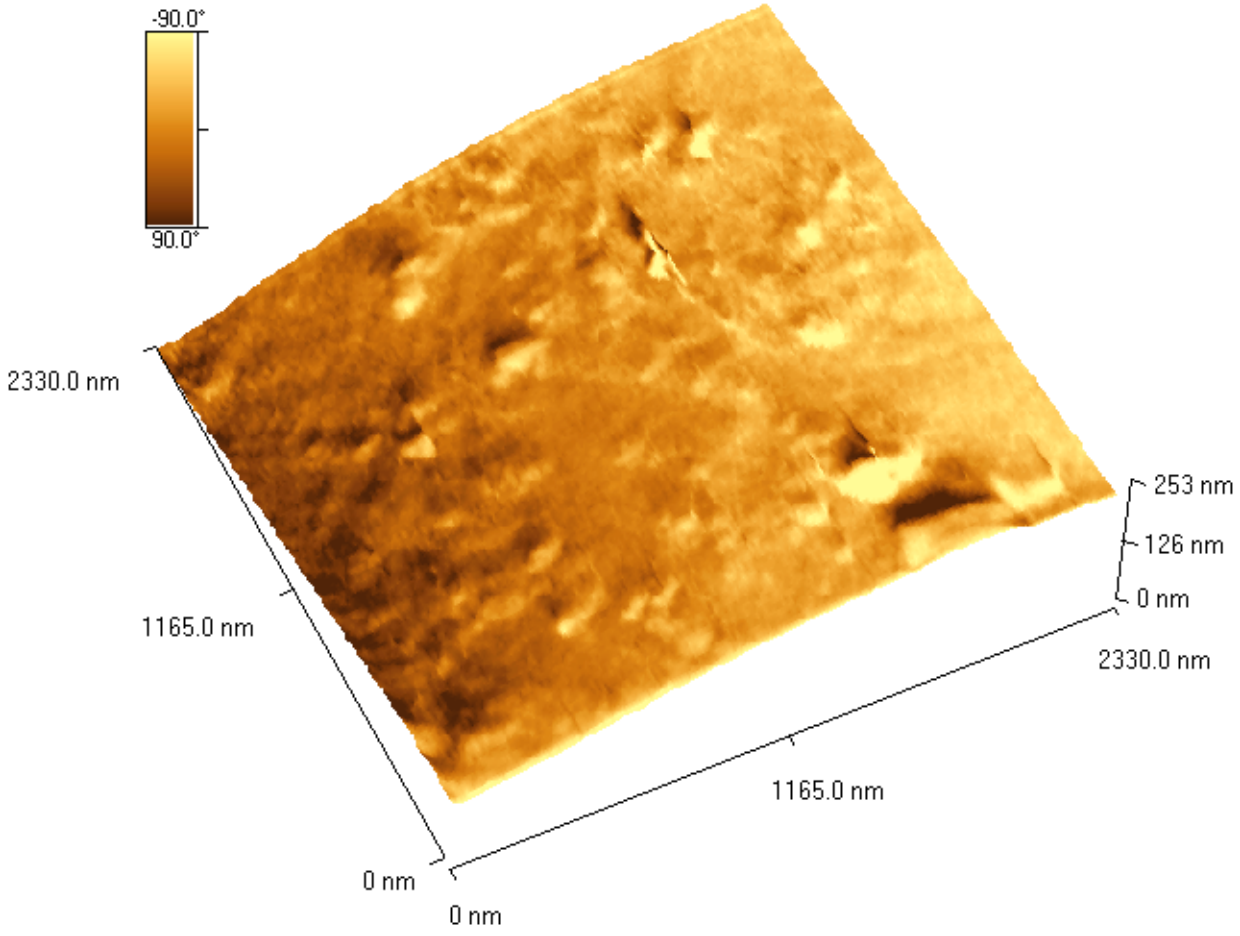

Figure 10. Large Range AFM Image of Glass Fiber

In making the scanning sample, an identification mark was made for individual fibers under the microscope with the micro-debonding apparatus. Using the larger scanner tip, it could be determined which fiber was good enough to take further AFM scanning. Thanks to the mark, the individual fiber could be identified by the camera mounted inside the AFM stage sensor, which made it possible to find the target fiber after changing of the scanner tip.

In one of the studies, fifteen broken fibers from one static tension test and fourteen broken fibers from one fatigue test were randomly taken from the broken specimens to make AFM samples. Mechanical test results for those fiber specimens are listed in Table 2. The stress values were determined from the maximum force and the measured number of fibers and average fiber cross-sectional area.

Table 2 Mechanical Test Results of Fiber Strands

Number of Fibers In Strands	Max. Loads Applied (Newton)	Tensile Stress on fibers (Mpa)	Cycles to Failure
124	102.3	3480	1
143	50.9	1740	59258

By scanning with the long range scanner, it was found that 11 fibers in the static specimen and 10 fibers in the fatigued specimen were good enough for further AFM scanning.

Overall, as shown in Appendix 1, among total 25 fibers from fatigue tests (from three fatigued specimens), 14 were found to have a scratch similar to that shown in Figure 12, but none of this kind of scratches were observed on 18 fibers from static tested specimens. Up to 10 positions were scanned on each fiber searching for damage. The fact that most fibers from fatigue tested specimens have scratches strongly demonstrates that the fatigue process causes scratches on fiber surfaces. The reason that only a fraction of the fatigued fibers had scratches might be attributed to the fact that the scratch can be made only on those fibers

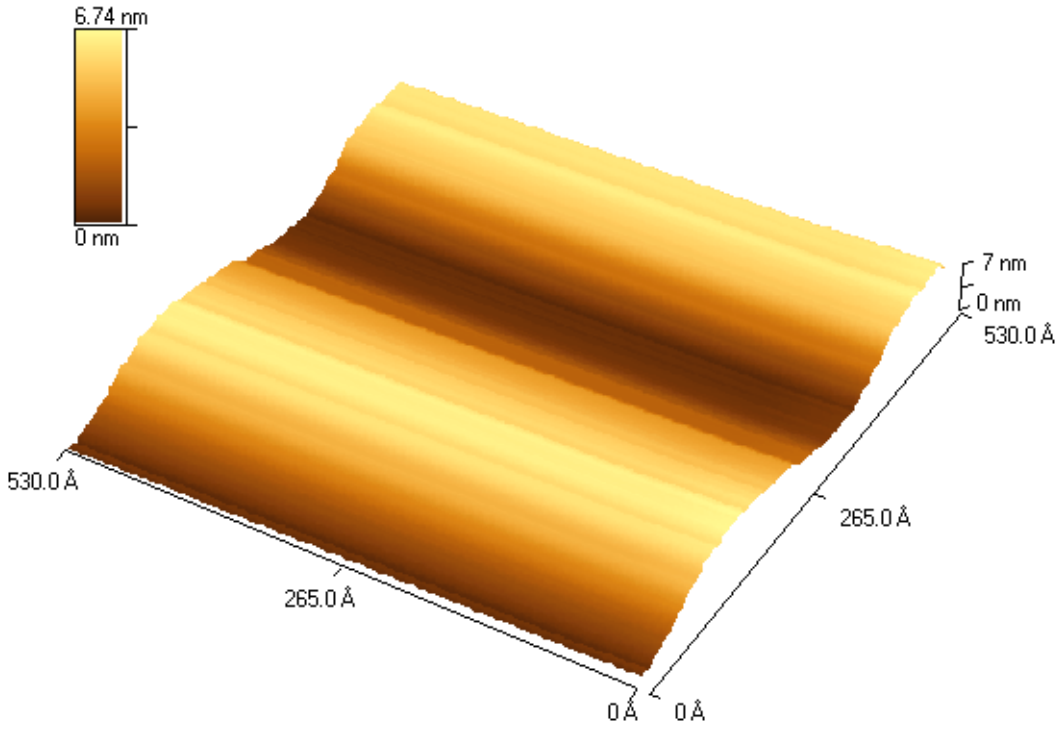

Figure 12. AFM Image of Fatigued Glass Fiber

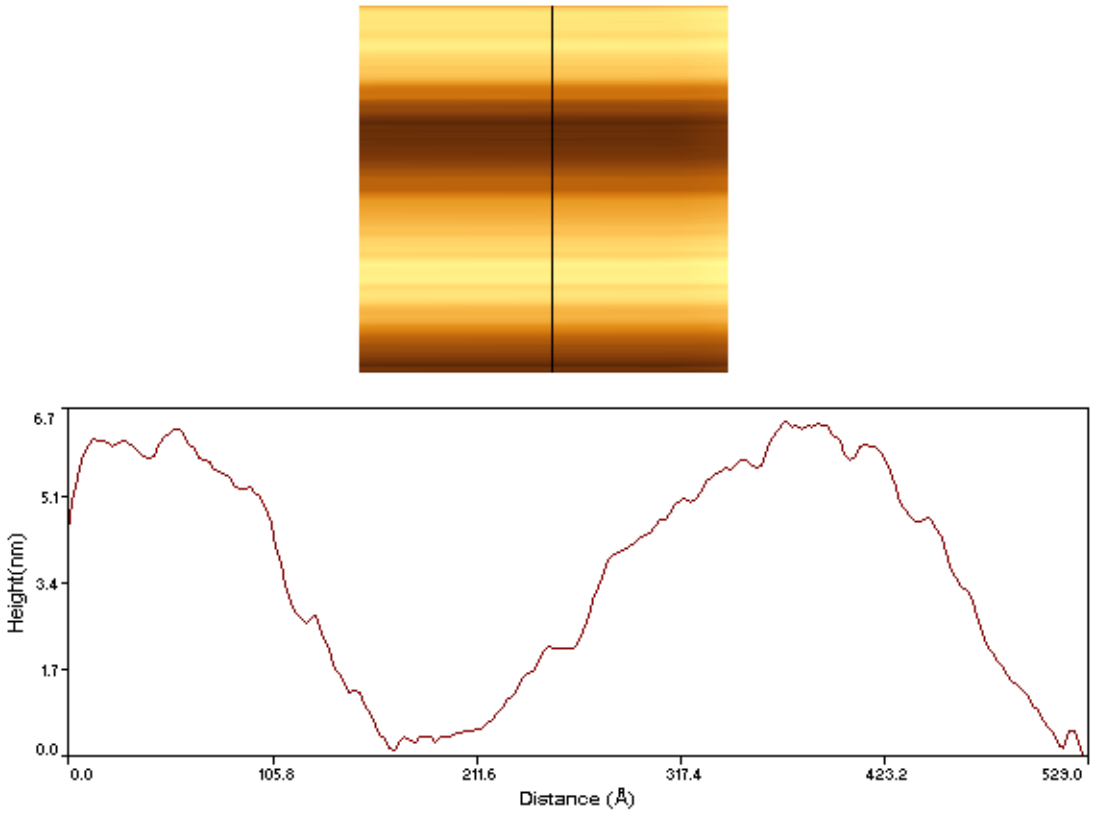

Figure 13. Profile of Cracks

which contact other fibers.

The size of the scratch can be calculated by the analysis software of AFM. The profile of the scratch is shown in Figure 13. It is found that the scratch measures about 6.7 nm deep.

Failed fibers in a fatigued specimen may have failed before total specimen failure (fatigue failures) or as part of the final failure process (static-like failures). The calculations show the expected range of actual flaw size for each case.

For a typical glass fiber, K_{IC} is 0.76 $MN/m^{3/2}$ [51]. The tensile strength of the fiber used in this study is about 3500 MPa while the fatigue stress on the fiber is 1740 MPa. Therefore, the size of crack can be calculated as [52]

$$a = [K_{IC}/(1.12\sigma)]^2/\pi = [0.76/(3500*1.12)]^2/\ 3.14 = 12.0 \text{ nm} \qquad \text{(static)}$$

$$a = [K_{IC}/(1.12\sigma)]^2/\pi = [0.76/(1700*1.12)]^2/\ 3.14 = \ 50.7 \text{ nm} \qquad \text{(fatigue)}$$

For AFM scanning, the maximum achievable resolution in the plane formed by the x and y axes is established by the geometry of the probe itself. When imaging extremely flat surfaces this is determined by the diameter of the atom at the probe tip. Thus, the macroscopic probe tip structure is not critical in atomic resolution imaging. When imaging large surface features, however, image quality is determined by probe geometry. The tip diameter and aspect ratio are critical , as shown in Figure 14 [53]. Because of the small size of the crack, it could happen that the probe can not reach the bottom of the crack. If the crack has the shape shown in part (a) of Figure 15, it is anticipated that the image could be that shown in part (b) of Figure 15. Therefore, it is reasonable to assume that the actual size of the crack might be larger than that shown in Figure 13.

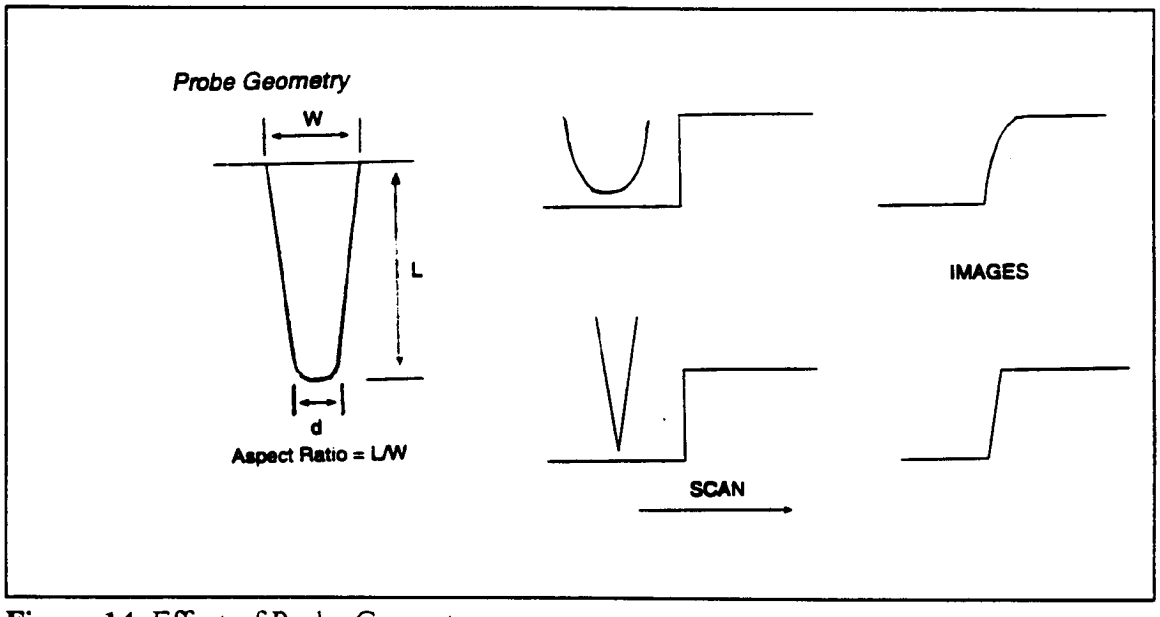

Figure 14. Effect of Probe Geometry

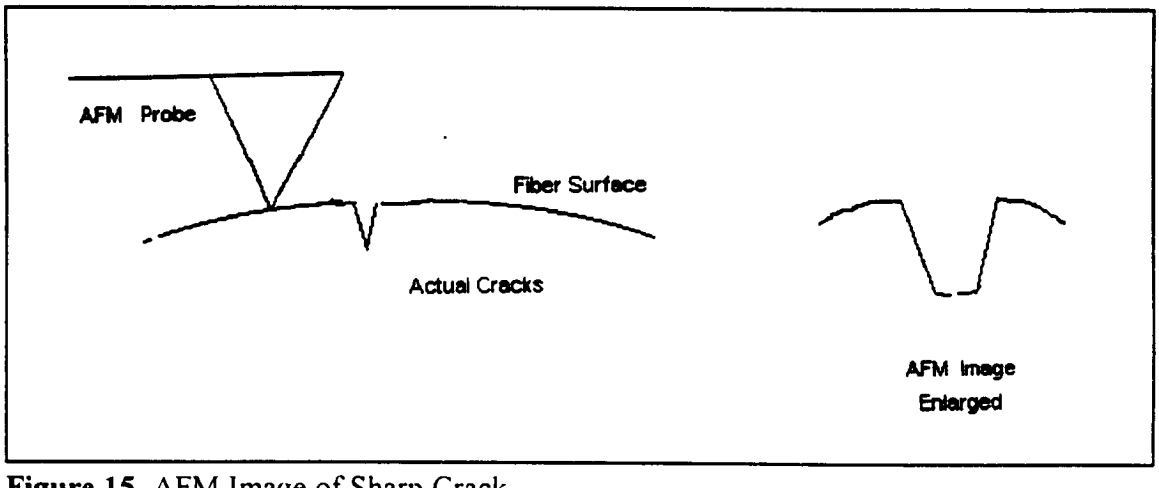

Figure 15. AFM Image of Sharp Crack

Considering the fact that the fatigued fiber has cracks which are of the same order of magnitude in depth to those calculated for failure, it can be concluded that the crack detected is probably the cause of final failure of the fibers and the composite. Therefore, the fatigue mechanism can be depicted as that of local contact of fibers resulting in damage at points

where fibers contact each other ; the damage to the fiber surface then weakens the fiber until it fails at the applied stress. In this study, the detailed nature of the damage and its depth has not been clearly established. However, significant damage has been observed on fatigued fibers, and it is likely that the largest scratches have not been observed. It is also likely that the fibers observed were not actually failed in fatigue, since most of the fibers fail as part of the final failure process in a sudden event.

Coating of Fibers

Effect of Graphite Content on the Fiber Surface

Three treatment slurries with different graphite content were used to treat the fiber strands. Their graphite contents were 1%, 3%, and 5%. Scanning Electronic Microscopy (SEM) was used to image the fiber surface and to evaluate the treatment effect. SEM images of these fibers are shown in Figures 16, 17, and 18. From these figures, it is observed that the fiber treated with 1% slurry was not completely coated with graphite while the other two fibers were completely coated. It seems that the 1% slurry is too dilute to be effective. It is also noted that the surfaces of fibers treated by 3% graphite slurry are smoother than those of fibers treated by 5% graphite slurry.

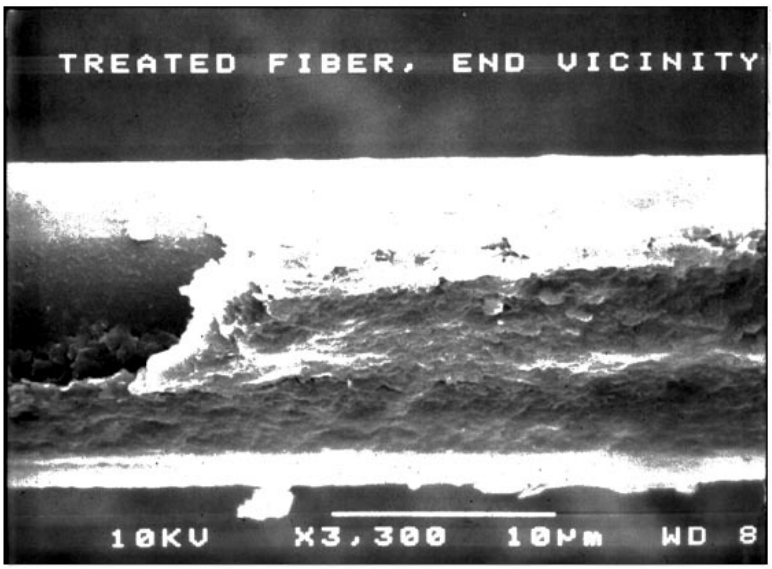

Figure 16. SEM Image of 1% Graphite Coated Fiber

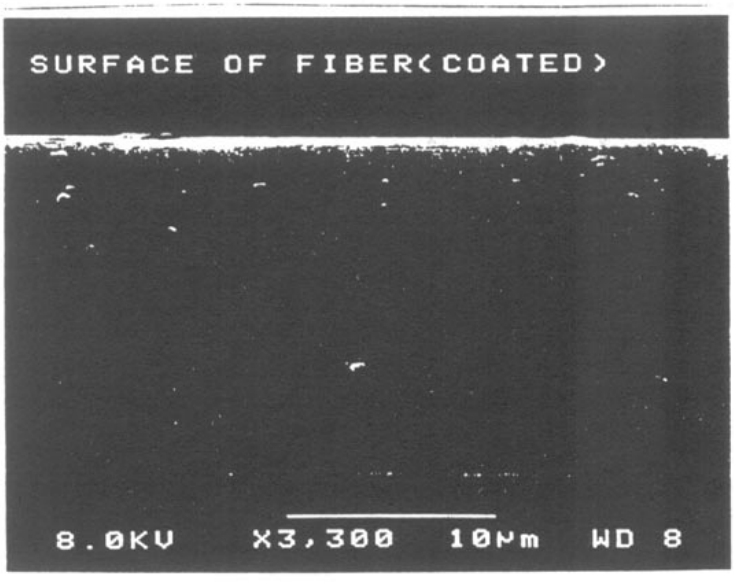

Figure 17. SEM Image of 3% Graphite Coated Fiber

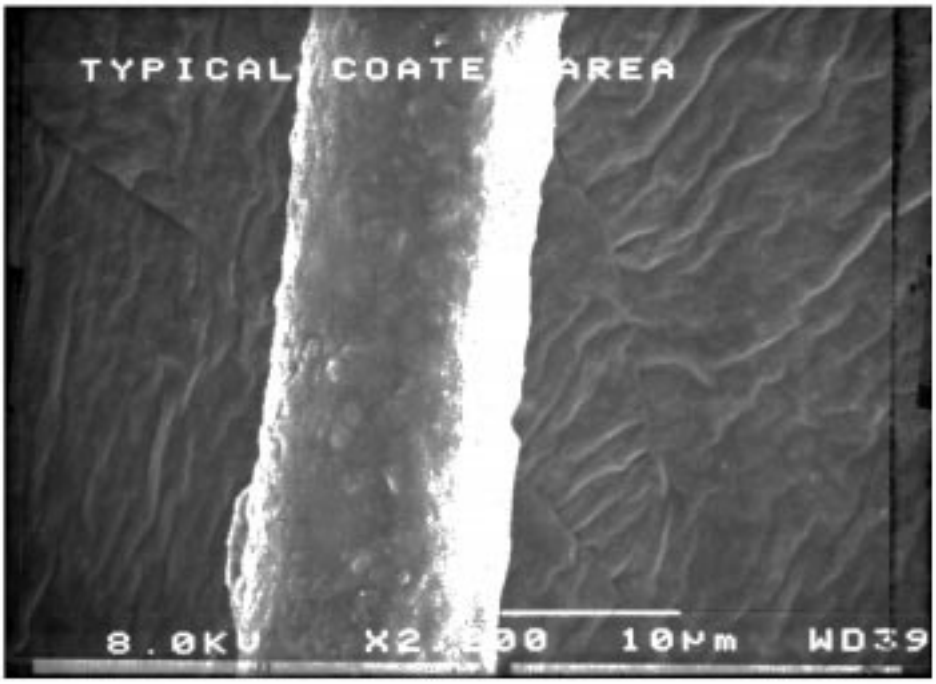

Figure 18. SEM Image of 5% Graphite Coated Fiber

Element analysis diagrams are shown in Figure 19 for coated fiber (coated by 3% graphite slurry) and Figure 20 for a control fiber. From these two diagrams, it was found that the surface consists mainly of carbon and oxygen for both coated or uncoated fiber. However, the relative element content is different. The detailed element analysis data is also listed in Table 3.

Table 3. Element Analysis of Coated Fiber and Normal Fiber

Element	C	O	Al	Si	Ca
Atom% **	92/44.58	7.59/41.37	0/2.36	8.38/8.24	3.45/0.02
Wt% **	89.26/32.83	9.81/40.59	0/3.90	0.85/14.19	0.07/8.49

** Coated Fiber/control Fiber

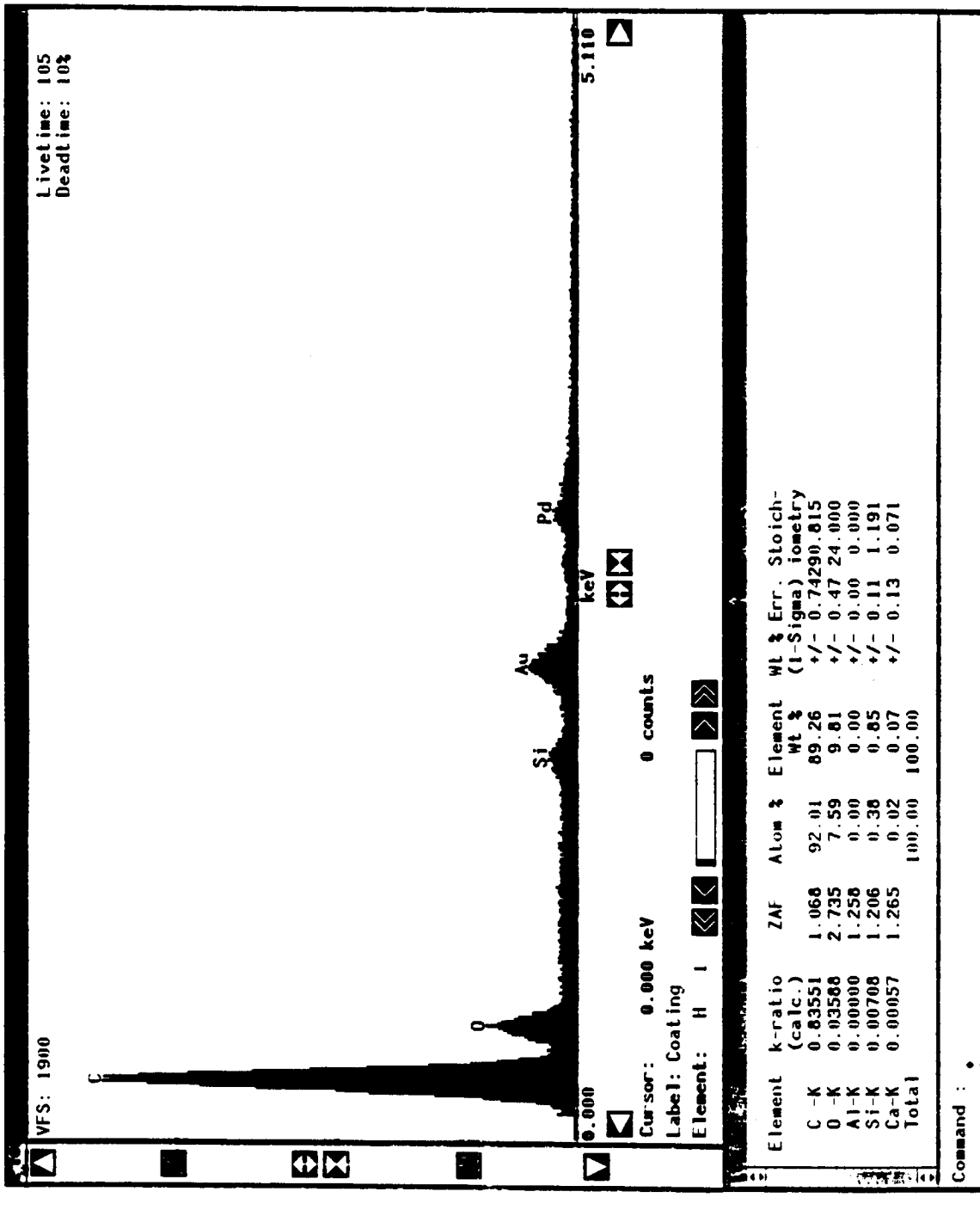

Figure 19. Element Analysis Diagram of Coated Fiber

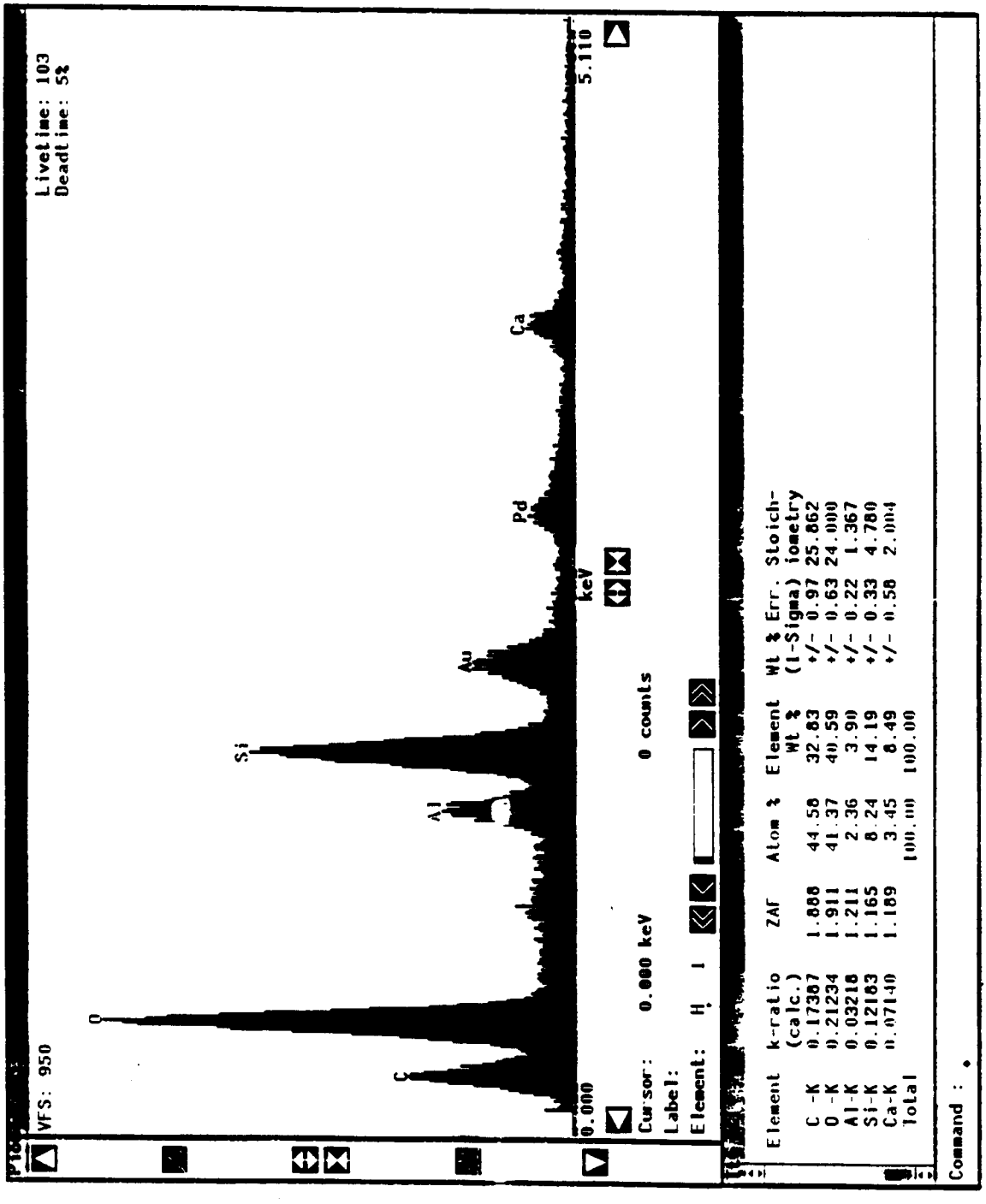

Figure 20. Element Analysis Diagram of Control Fiber

From Table 3, it is found that after coating, the carbon content increases from 45% to 92% by atom or from 33% to 89% by weight.

X-Ray Photoelectron Spectroscopy (XPS) was used to study state of carbon on the fiber surface. The XPS carbon spectrum of coated fibers is shown in Figure 21 and that of as-received fibers in Figure 22. The carbon peak for the as-received fiber is symmetric, which means that the carbon is in a single combined state. The carbon peak of the coated fiber is unsymmetric. This unsymmetry resulted from the graphite slurry used to coat fiber. Therefore, the increased carbon content for coated fiber can be attributed to the graphite added.

The strand composite made from fiber coated by the 3% graphite slurry was used to prepare 90^0 tensile test specimens, that is, specimens with the fibers oriented perpendicular to the stress direction. Specimens in this orientation fail by cracks growing parallel to the fiber in the matrix and interface. Thus, they produce fracture surfaces which are convenient for observation of the interface. The failure surface was scanned with SEM. The SEM micrograph shown in Figure 23 indicates some graphite remaining on the surface of fibers in the composite.

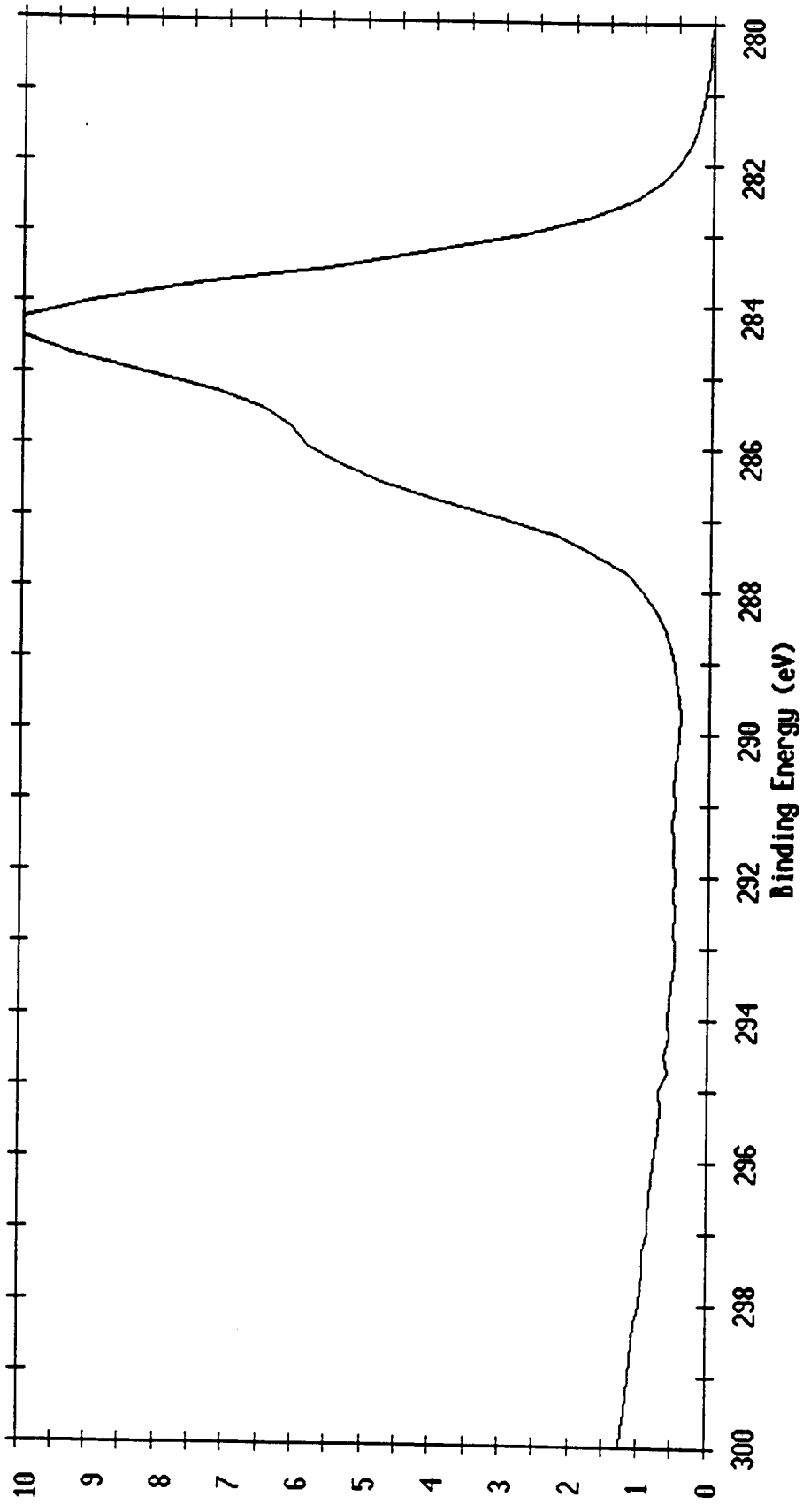

Figure 21. XPS Carbon Spectrum for Coated Fiber

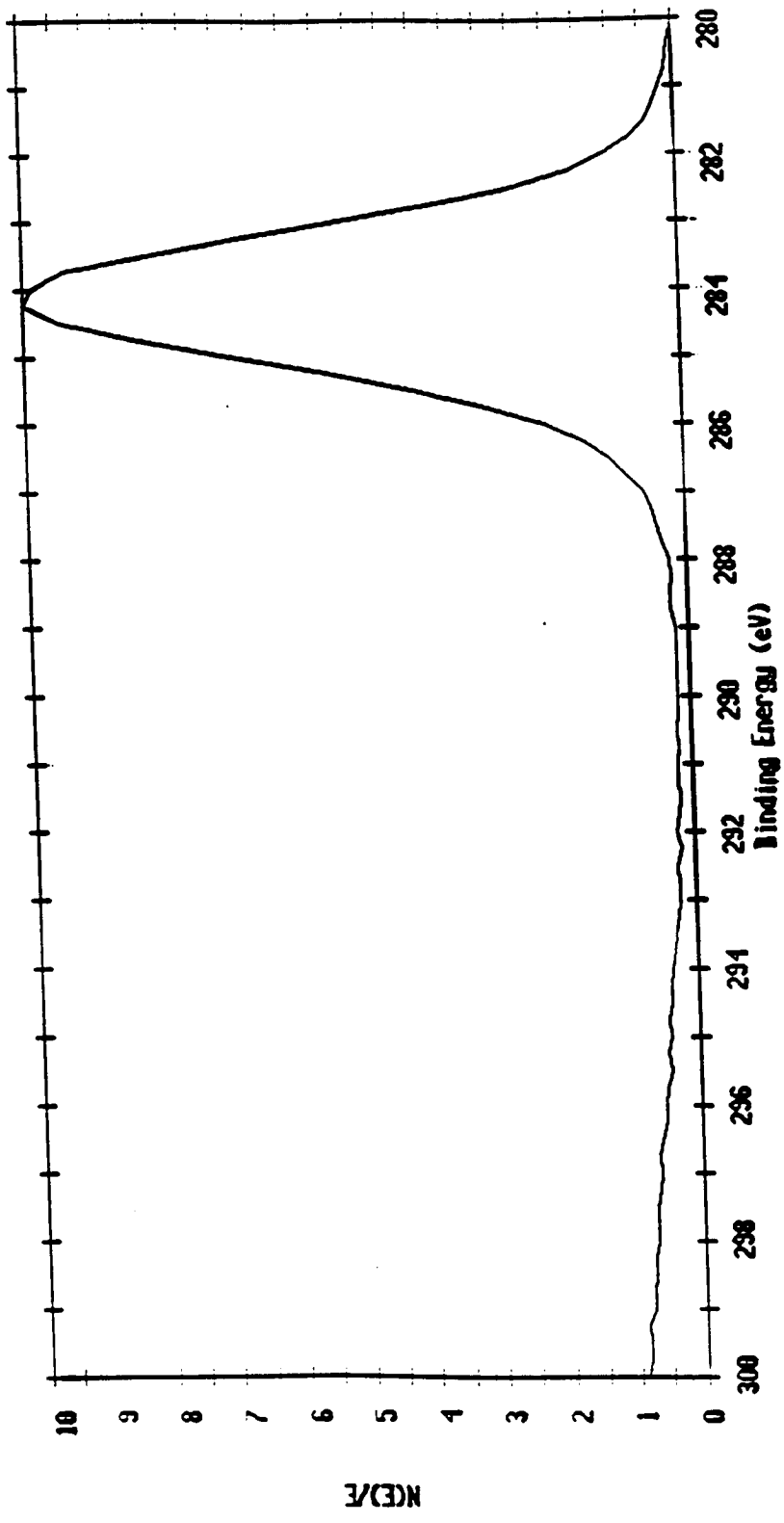

Figure 22. XPS Carbon Spectrum for As-received Fiber

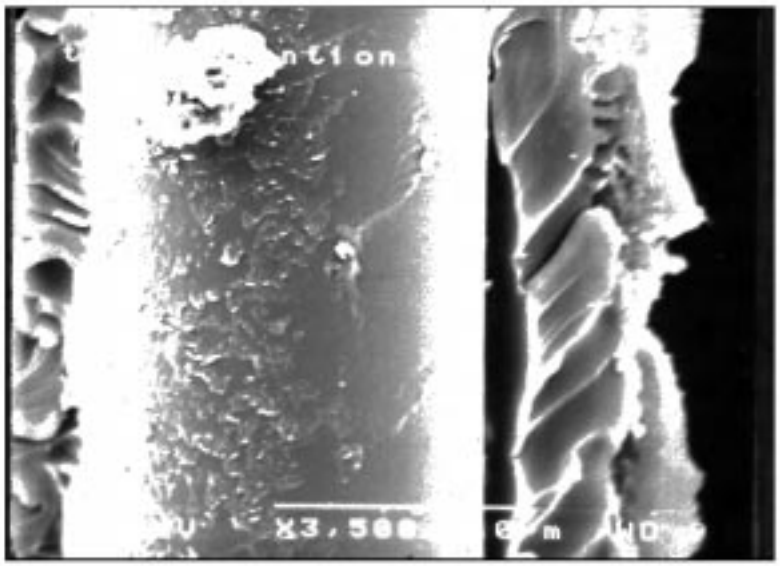

Figure 23. SEM Micrograph of Coated Fiber on Fracture Surface After Transverse Tensile Test

Establishment of Fatigue Test for Strand Composites

Effect of Silicon Rubber On Static test

The strand composite tensile specimen was prepared by two different methods. The sole difference between them is that silicon rubber is used only in one as shown in Figure 9. The static strengths obtained from both methods are listed in Table 4.

Table 4 The Effect of Silicon Rubber on Static Tensile Strength (Tensile break Load)

		Tensile Break Forces (Newtons)				
Table Type	# of Specimen	1	2	3	4	5
Tab with Silicon Rubber		277.6	282.4	285.1	263.3	296.7
Tab without Silicon Rubber		273.6	278.9	259.3	293.1	298.9

The Paired two sample T-test was used to test if there is a significant difference between the two groups of specimens. The t was calculated to be 0.85 , which is less than critical t

value of 2.765 for degree of freedom DF=4, and confidence level α=0.05. Therefore, it can be concluded, with 95% confidence, that the difference between these two methods for static strength is not significant.

The photograph of a broken specimen is shown in Figure 24 (a). It is found that the strand is broken in the middle section of the specimen. Therefore, for the static test, tabs with or without rubber are acceptable.

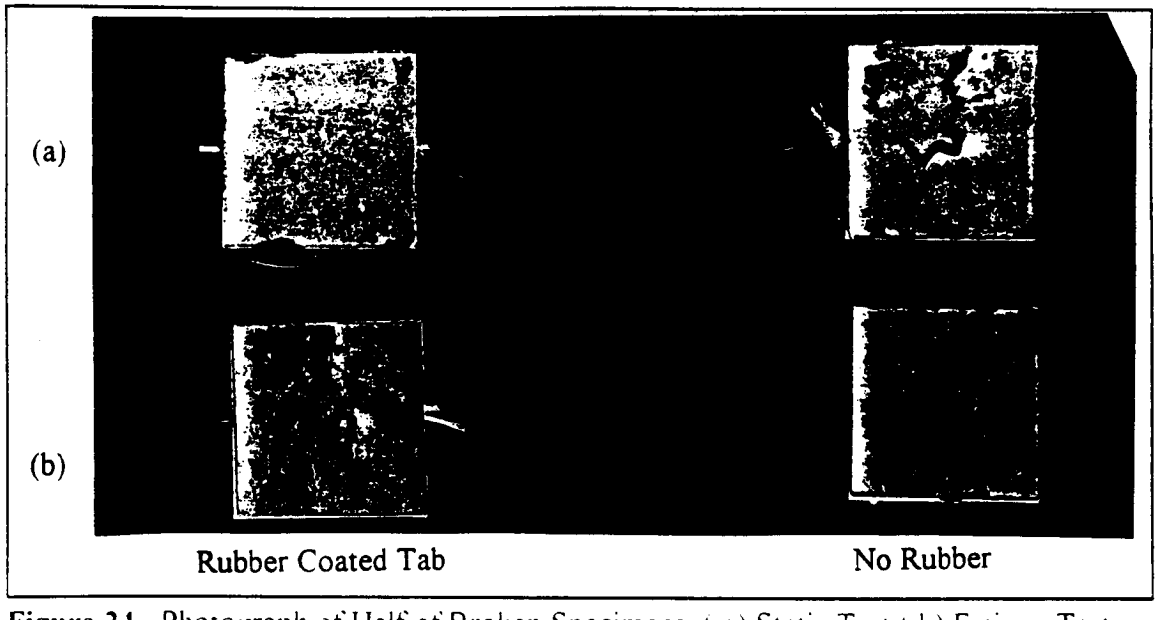

Figure 24. Photograph of Half of Broken Specimens (a) Static Test (b) Fatigue Test With and Without Rubber Coated Tabs

Effect of Silicon Rubber on Fatigue Test

A broken specimen after fatigue testing at 50% stress level is shown in Figure 24 (b). The cycles to failure was 2968 for the specimen made from tabs without rubber, but 925,877 for the specimen made from tabs with rubber. It was found that specimens with rubber coated

tabs break in the middle of the specimen while those using tabs without rubber break near one of the tabs. Thus, rubber is used with the fatigue specimens.

The fatigue diagram for specimens of control fiber strands with and without rubber-coated tabs is shown in Figure 25. At 50% load level (S/So=0.5), typical fatigue to failure cycles is about one hundred thousand for rubber-coated tab specimens and only about two thousand for specimens from tabs without rubber.

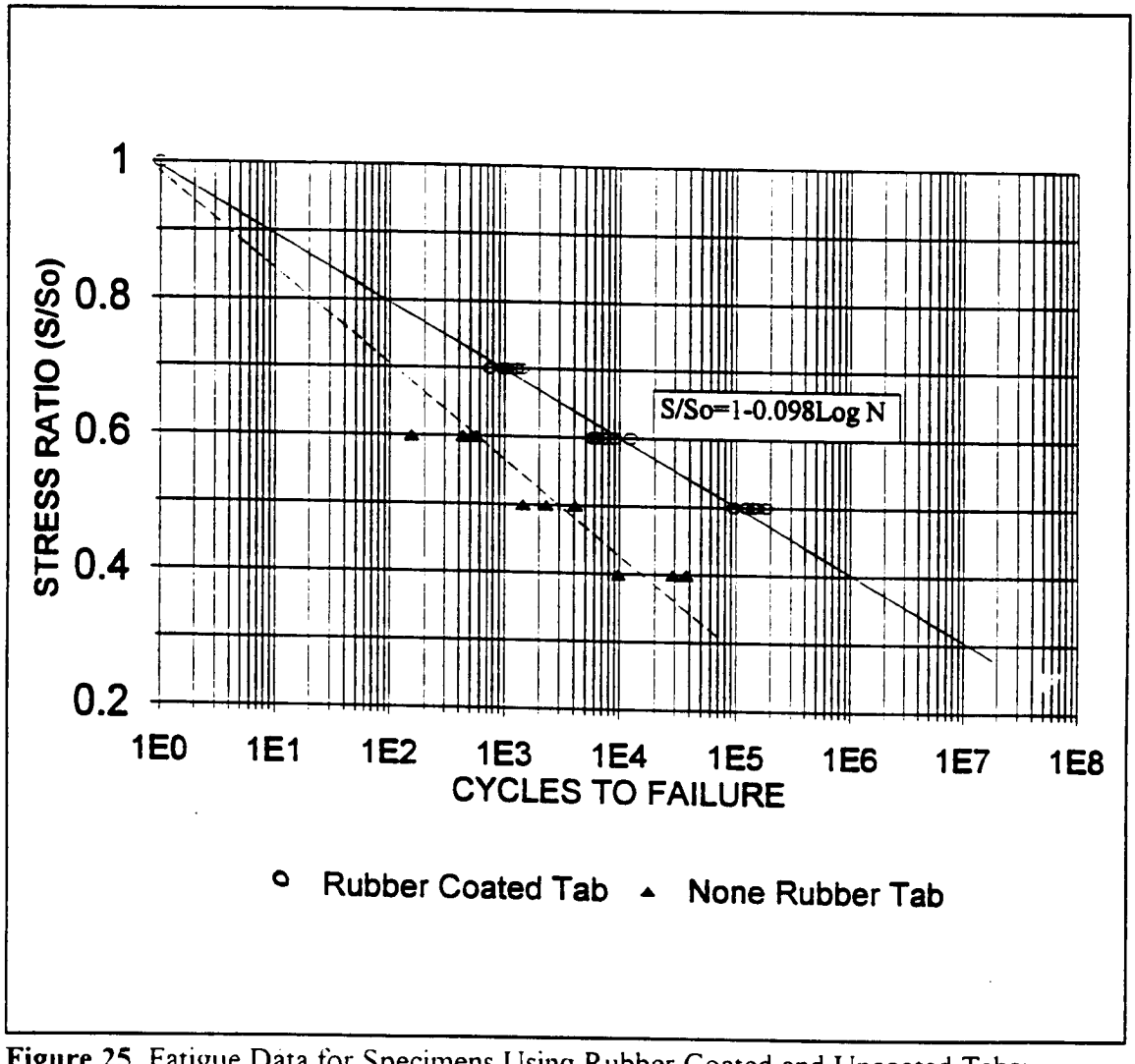

Figure 25. Fatigue Data for Specimens Using Rubber Coated and Uncoated Tabs: As-received Material, R=0.1

The data are fit with a straight line, giving a fatigue S-N relationship

$$S/So=1.0-b*\log N \quad (1)$$

where S is the maximum cyclic stress, So is the static strength, N is the cycles to failure and b is the slope of the S-N curve, or the fatigue coefficient.

The rubber-coated tab specimen fatigue degradation rate is 0.098, which is good agreement with literature values [54]. For well aligned E-glass composites such as strand composites, the best fatigue rate is about 0.10, which means that the strand composite fatigue test method established in this study is satisfactory.

Effect of Surface Treatment on Static Tensile Strength

The control polyester/glass-strand composite and the polyester/coated glass-strand composite tensile strength have been determined. The control glass strand is passed through a solution with the same other components but no graphite as compared with that for coating the fibers. Because it is difficult to accurately measure the cross-sectional area of the strand composite, and because the composite tensile strength is mainly determined by the fiber type and its volume content [55], the tensile breaking force is used to compare their strength , rather than the stress. Strand composites with the same number of fibers and similar resin content will sustain the same breaking force. Since all the strand specimens were cut from one long fiber strand, it is reasonable to assume that they have the same number of fibers.

To verify the consistency of the specimens, five five-inch-long strands were randomly taken from one long strand and tensile tested. Their breaking loads were 62.4, 63.5, 64.1, 59.2, 66.7 lb. The calculated coefficient of variation is 4.3% , which is less than 5%, the value required by ASTM 2343, "Tensile Properties of Glass Fiber Strands, Yarns, and Rovings

Used in Reinforced Plastics" [56] . Therefore, it is reasonable to believe that these specimens are consistent when prepared in this manner.

The tensile breaking load of the control strands and two different types of coated fiber strands were determined. The difference between the two coated fibers is that the one was treated with 3% graphite slurry and the other was treated with 5% graphite slurry. The results are listed in Table 5.

Table 5. The Effect of Coating on Strand Composite Static Tensile Strength

Coating	Tensile Break Force (Newton)					**Average**
Control	277.6	282.4	285.1	263.3	298.8	**281.1**
3% Graphite Slurry	186.2	269.1	276.2	260.2	285.6	**278.0**
5% Graphite Slurry	234.9	242.0	250.0	221.0	248.2	**238.9**

Statistically, the one-way classification analysis for the data listed in Table 6 shows that the calculated F value is equal to 16.03, which is higher than the critical F, 3.88, for α=0.05 and DF= 12. Therefore, the effect of coating on tensile strength is significant with 95% confidence. The Two-sample T test was further used to determine the extent of this difference. The calculated t value for samples from controlled and 3% graphite treated fibers is 0.589 while that for samples from 3% and 5% graphite fibers is 4.06. The critical t value, $t_{df=4,\ \alpha=0.05}$ is 2.78. Therefore, it can be concluded that, with 95% confidence, the difference between control fiber and 3% graphite coated fiber is not significant while the 5% graphite coated fiber tensile strength is significantly lower than either of the others.

The lower tensile strength of the 5% graphite slurry strands can be attributed to their rough surface as shown in Figure 19. The rough coating surface will result in some non-uniform cracking on the fiber surface, which will decrease fiber strength. Similar results were

also observed by Ochiai [57].

Because the fiber coated with 3% graphite slurry has a smother surface and the same tensile strength as that of the control fiber, this fiber was selected for further study.

Effect of Coating on Strand Composite Interface Strength

The micro-debonding load depends not only on the interface strength but also on the space between the target fiber and its nearest neighbor fibers. A typical cross-section of strand composite is shown in Figure 26, where the fiber with a triangular mark at the end was debonded. The dark circle surrounding that fiber is the debonded area. For consistency, fibers with almost the same diameter and spacing to the nearest-neighbor fiber were selected for testing. Therefore, the debonding load can be used directly without data reduction to compare the interface strength for as-received fibers, control fibers, and coated fibers. The microdebonding forces are shown in Table 6.

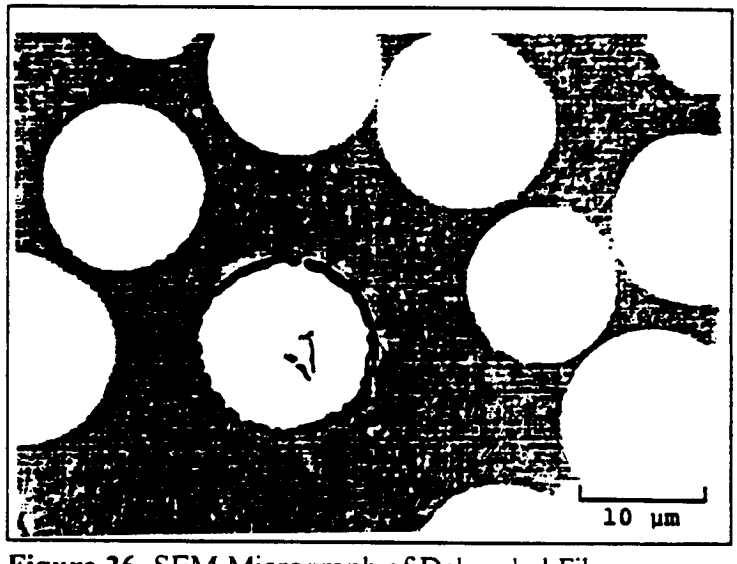

Figure 26. SEM Micrograph of Debonded Fiber

Table 6. The Microdebonding Force For Different Fibers (Grams.)

	Test No.								**Sample**
Fibers	1	2	3	4	5	6	7	8	**Average**
As-received Fibers	9.0	11.0	13.0	11.8	12.0	9.8	10.2	11.0	**11.0**
Control Fibers	13.5	15.5	12.2	8.8	10.0	10.0	11.2	11.0	**11.5**
Coated Fibers	10.0	12.5	9.2	9.2	11.0	11.0	8.0	8.6	**9.9**

From Table 5, it seems that the control fiber average micro-debonding load is 4.6% higher than that of as-received fibers, while the coated fiber average microdebonding load is 9% lower than that of as-received fibers. Variance analysis was used to determine whether this difference is significant. The null-hypothesis is:

Ho: there is significant difference between different fibers

H1: there is no significant difference between different fibers

The calculated F value is 1.126. For α=0.05, with degree of freedom, DF=16, the critical $F_{0.05,16}$ equals to 2.657.

Because $F<F_{0.05,16}$, the null-hypothesis can not be rejected. Therefore, with more than 95% confidence, it can be stated that there is no significant difference among the micro-debonding loads of the three different fiber treatments.

Fatigue Resistance of Coated Fiber Strands

The fatigue resistance of coated fiber strand (3% graphite particle slurry), control fiber strand , and as-received fiber strand composites was determined by the fatigue test method described earlier. The fatigue resistance was calculated by a fit to Equation 1. The fiber volume fraction was about 0.60.

In the present study, force instead of stress is used to calculate the b value for strand composites . The static tensile strength is listed in Table 7.

Table 7. Static Tensile Strength ,So, of Coated, Control, and As-received Strands

		Tensile Strength (Force, Newton)					
Type Of Strands	# of Specimen	1	2	3	4	5	**Average**
Control		277.6	282.4	285.1	263.3	298.8	281.1
As-received		259.8	279.3	305.9	276.2	266.0	**277.4**
Coated		281.1	265.1	257.1	282.4	290.9	**275.3**

One-way variance analysis was again used here to compare the static strength. The calculated F value is 0.206, which is less than critical F value, $F_{\alpha=0.05,\ df=12} = 3.88$. Therefore, there is no significant difference in static tensile strength between coated, control, and as received strands.

The strand composite cycles to failure at different maximum stress levels are listed in Appendix 2. The corresponding S-N curve is shown in Figure 27. Figure 27 shows that the fatigue coefficient is 0.098 for as-received fiber and control fiber strands, similar to the expected value of 0.1 described earlier. The fatigue coefficient for 3% graphite coated strand composite is 0.071, lower than that of the other composites. This fatigue resistance improvement is significant. At S/So=0.5, with the maximum stress at half of the static strength, the as-received and control strands can only sustain about 0.1 million cycles , while the graphite coated fiber strand can sustain about 10 million cycles, giving approximately 100 times longer lifetime.

Because there is no difference in fatigue coefficient for as-received fiber and control fiber strands, it can be concluded that the coating procedure itself brought no difference to the composite strength or fatigue resistance. As mentioned above, the only difference between control fiber and coated fiber is the graphite added into the coating mixture for the coated fiber. It is reasonable to credit the fatigue resistance increase in the coated fiber strands to the graphite at the interface. It is postulated that because of excellent lubricity of the graphite, the fretting effect was significantly decreased and thus the surface damage at the contact site was reduced. Therefore, this improvement is also evidence of contact damage fatigue mechanism.

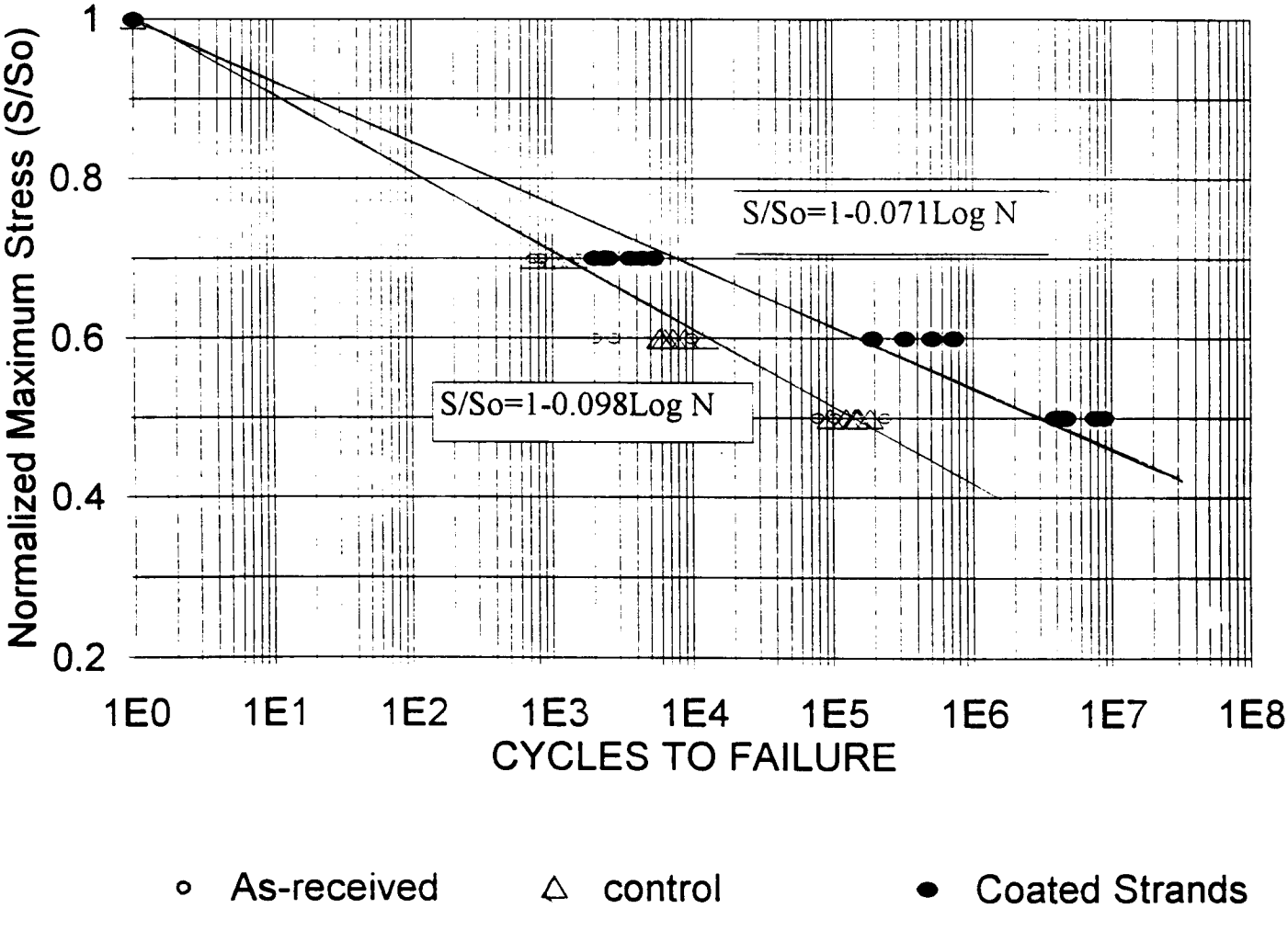

Figure 27. S-N Curves for Glass Fiber Strand Composites With and Without Fiber Coatings, R=0.1

Fatigue Resistance of Coated Fabrics

The increase in fatigue resistance is important only if the treatment can be economically competitive and industrially acceptable . It might be economical if fabrics rather than single strands could be coated, so a study of fabric coating was also carried out. The coated fabrics were then made into composites by the RTM method. The high-frequency-fatigue testing method established at MSU was used to test the fabric composite fatigue resistance.

The tensile fatigue test data for as received fabrics and that cited from database [58] are listed in Appendix 3. The same raw material and test procedure as used to establish the database was used in this study. The tensile fatigue test data for control fabrics and coated fabrics are also listed in Appendix 3.

From these data , the average static tensile strength is calculated to be 1367 MPA . As compared with database static strength, 1502 MPa , the difference is within acceptable range of experimental error for different batches.

As-received fabric and database tensile S-N curves are shown in Figure 28. The fiber volume fraction is 61% for the former and 67% for the later. The data obtained in this study fit the database very well. Both have fatigue coefficient of about 0.13 per-decade. Therefore, the test procedure was run correctly.

Control and coated fabric unidirectional composite S-N curves are shown in Figure 29. This Figure shows that the control fabric has the same degradation rate as the as-received fabric, while the coated fabric fatigue coefficient is about 0.089, which means that coated fabric can sustain about 10 million cycles at S/So=0.4. The as-received fabric can only sustain less than 0.1 million cycles at this stress. The high value of b relative to strands is typical of

fabrics at high fiber contents [58]

Two batches of coated fabric specimens were used to test whether there were differences between batches. Their S-N curves are shown in Figure 30. It is clear that there is no significant difference between different replications.

E-glass strand composites have better fatigue resistance than do stitched fabric composites. This is true of both coated and control cases. The reason for this is not clear, but may relate to fabric stitching and heterogeneous structure of the stranded fabrics. Results in the MSU/DOE database show a higher b for fabrics above about V_f=0.49. The cause of this is under investigation.

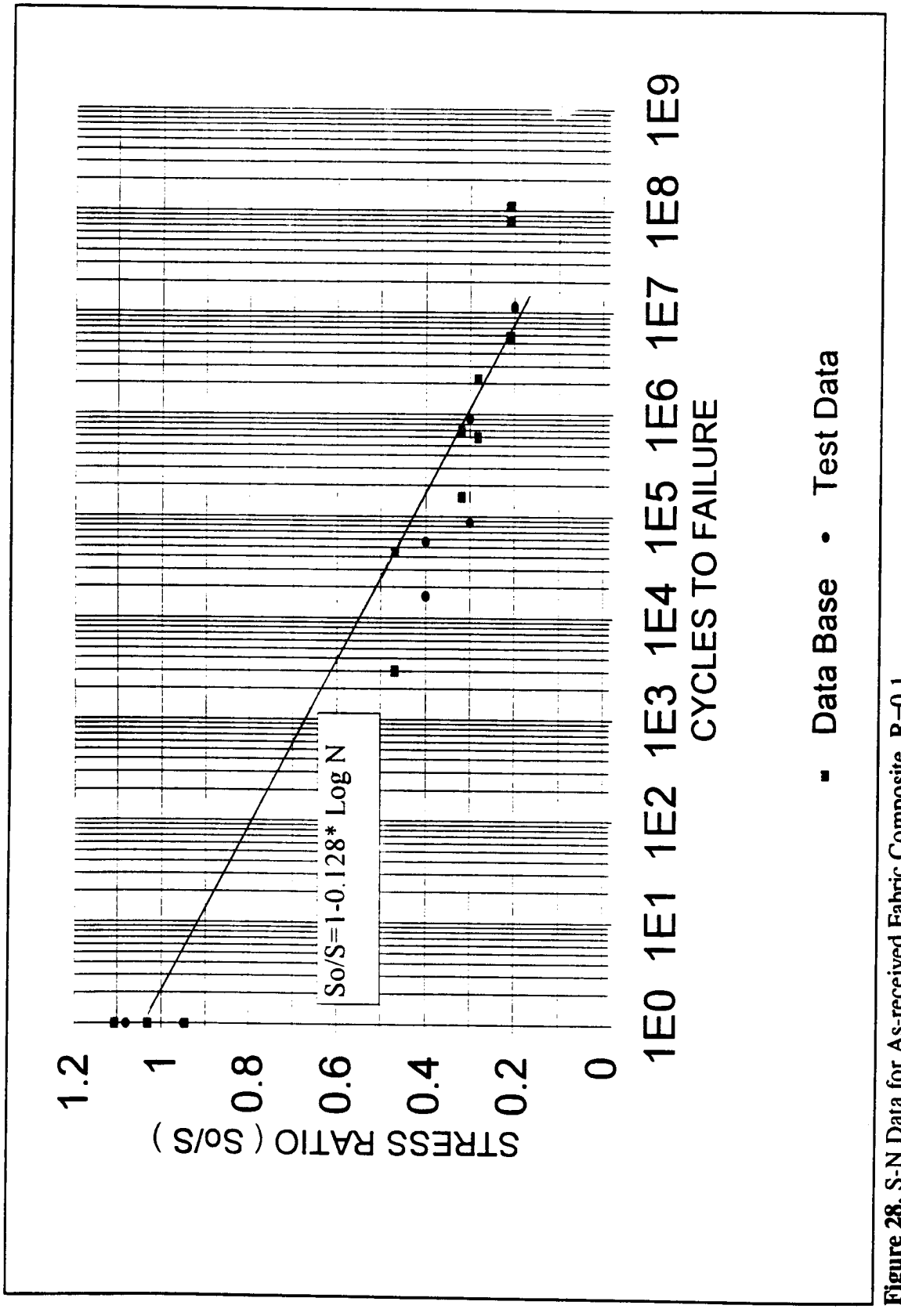

Figure 28. S-N Data for As-received Fabric Composite, R=0.1

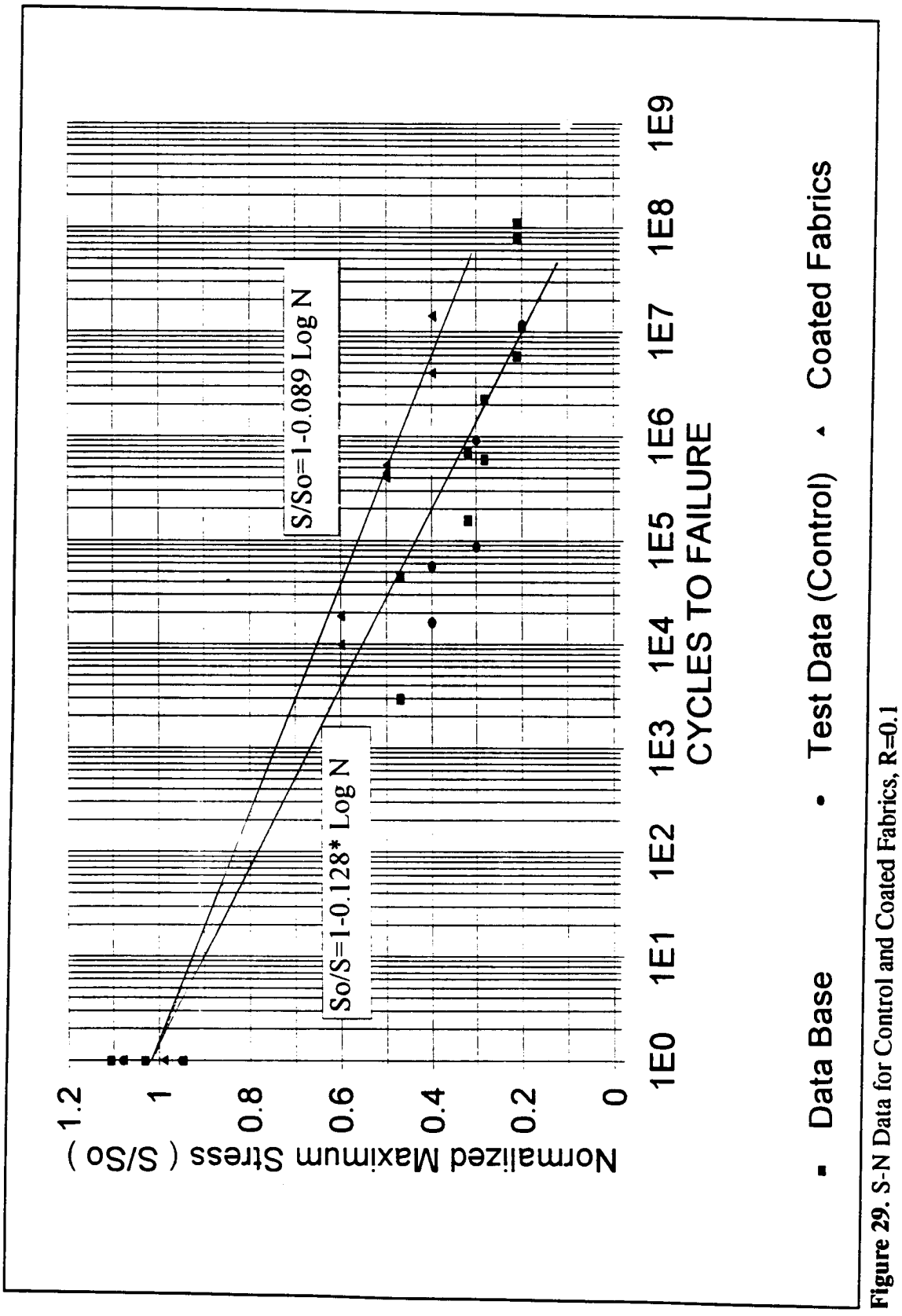

Figure 29. S-N Data for Control and Coated Fabrics, R=0.1

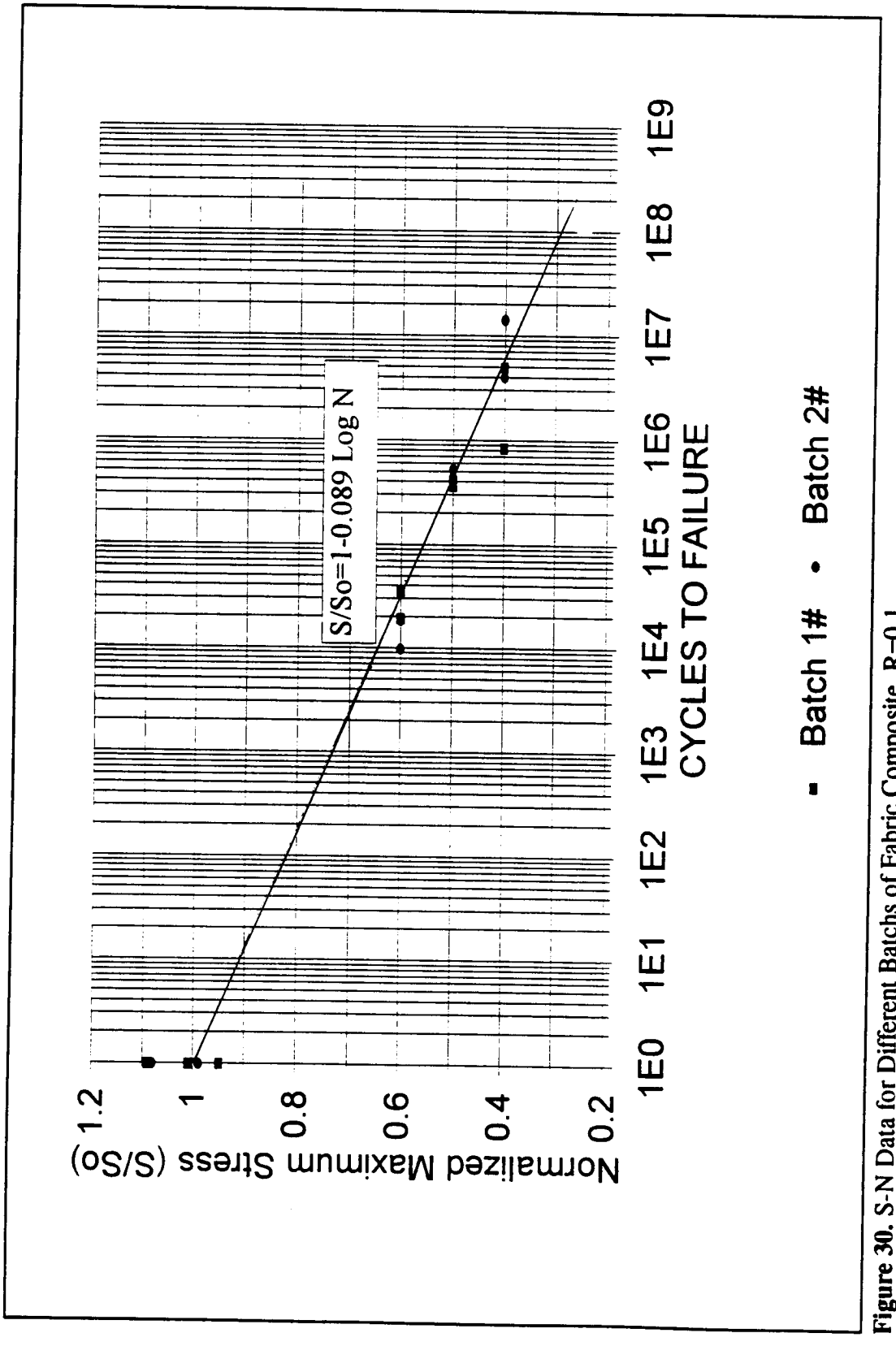

Figure 30. S-N Data for Different Batchs of Fabric Composite, R=0.1

CHAPTER FIVE

CONCLUSIONS AND RECOMMENDATIONS

Conclusions:

1) The high frequency tensile fatigue test method developed for small strand composites produced valid fatigue failures in the gage section. It was found that coating tab with silicon rubber is essential for fatigue testing but not for static testing. The fatigue coefficient, b, for as-received composites was 0.098 which is close to the 0.10 expected from the literature for well aligned glass strand composites. Thus, the test method is successful, and provides for high-frequency testing of small volumes of material. This is of practical significance for studies such as fiber coatings.

2) Atomic Force Microscopy provided useful images of surface damage on individual fibers. Significant scratches on fiber surfaces from fatigue tested specimens were found, but no scratches were found on static tested specimens. These scratches are concluded to be caused by the fatigue process, and are deep enough to cause fiber weakening.

3) A method of coating the fiber surface with graphite particles was established. SEM and verified graphite in the coating. It was found that a 3% graphite slurry in alcohol can be used to satisfactorily coat the glass fiber in the form of strands or stitched fabrics. Microdebonding testing was used to monitor the interface strength change as a result of coating. Statistical analysis of the results showed that, with 95% confidence, there is no significant difference in the bond strength of as-received, control, and coated fibers.

4)The graphite particle coated strand composites showed a static ultimate tensile strength which was not significantly different from the as-received or control strand composites. The

tensile fatigue coefficient, b, of as received and control strand composites was about 0.10, similar to the best quality fiberglass composite data in the literature. The coated strand composites were more fatigue resistant, with a b value of 0.071. This improvement is significant; at S/So= 0. 5, the cycles to failure is about 0.1 million for as-received strands but about 10 million for coated fiber strands. This 100-fold improvement is postulated to be caused by the graphite particles helping to resist surface damage to the fibers.

5) Stitched fabric composite tensile fatigue S-N data were obtained by an established high frequency fatigue test method, and the data for as-received fabric were consistent with the established database at this relatively high fiber volume fraction of 0.61. The glass fabrics were also successfully coated by the same coating mixture as used in strand coating. The coated fabric fatigue coefficient of 0.089 is significantly lower than that of the as-received fabrics, which were 0.128. This improvement is also significant, with a 100-fold increase in lifetime at S/So= 0.5.

6) The simplicity and low cost of the coating method established in this study shows good industrialization potential.

Recommendations:

1) In this study, atomic force microscopy in the contact mode was used. In low magnification scanning, the scanner arm was usually interfered by the fiber because of its curved shape; additionally, the magnification of positioning using the optical microscope within the AFM is too low to precisely move the scanner to a target area of less than 0.01 square micrometers. Therefore, in order to obtain better scanning results, the following

improvements are recommended:

a) a special scanner with longer leg

b) noncontact AFM scanning mode

c) more sophisticated AFM which can be used in an SEM to allow better positioning.

2) Additional tensile fatigue tests should be run at different conditions in order to obtain a complete fatigue spectrum, which is important for potential use in industry. The following experimental parameters are recommended:

a) at different stress levels, R= 0.05, 0.1, 0.2.

b) at different frequencies, 10, 20 50, 100 HZ.

c) at different maximum stresses, S/So= 0.7, 0.6, 0.2 for fabric composites.

S/So= 0.8, 0.3, 0.2 for strand composites.

3) In the strand composite fatigue test established in this study, the highest test frequency was 20Hz, which is still inconveniently low for low S/So fatigue tests, especially for the specimens with improved fatigue resistance. The main obstacle to achieving higher frequency tests is that for the testing machine used in this study, high frequency load control is not accurate enough when the load is lower than 10% of the load cell full range. The typical tensile breaking load of the strand composite is about 60 lb. Therefore, a load cell with a full range of about 200 lbs should be used to run fatigue test at S/So=0.3 with high frequency.

4) Although the coating method established in this study can effectively increase the tensile fatigue resistance of glass fiber composites, the fatigue resistance is still lower than that of

carbon fiber composites. To the knowledge of author, the most suspect factor is the channels formed between fibers. The thickness of coating is affected by the size of the channel, especially if the coating media is a liquid and the coated area can not be dried immediately. The following methods are recommended:

a) gas coating media such as plasma coating or CVD (Chemical Vapor Deposition)

b) a simple apparatus which can coat single fibers, dry the coating, and bind the coated fibers immediately after coating

5) Even without further improvement, commercialization of this method should be explored

REFERENCES

1. D.Bhagwan, Agarwal, Analysis and Performance of Fiber Composites, John Wiley & Sons, INC., Chapter 2, 1994.

2. Committee on Assessment of Research Needs for Wind Turbine Rotor Materials Technology, Assessment of Research Needs for Wind Turbin Rotor Materials Technology, National academy Press, Washington, D.C., 1991.

3. J.F.Mandell, D.D.Hung, and F.J.McGarry, "Tensile Fatigue of Glass Fiber Dominated Composites", Composites Technology Review, Vol.3, 93, 1981.

4. "Life Predication Methodologies for Composites Materials," Report of the Committee on Life Predication Methodologies for Composite Materials, National Materials Advisory Board, NRC, National Academy Press, Washington, D.C. !990.

5. A.H. Chardon and G. Verchery, Durablity of Polymer Based Composite System for Structure Applications, Elsevier Applied Science, London, 1991.

6. J. Schijve, "Significance of Fatigue Cracks in Micro-range and Macro-range" ASTM STP 415, P415,1967.

7. W. J. Plumbridge, J. Mat. Sci., 939, 1972.

8 Liu, H. W. And Iinno, N., " A Mechanical Model for Fatigue Crack Propagation." Fracture, p812, 1969.

9 Abdelsamie Moet, "Fatigue Failure." Chapter 18 in Failure of Plastics Edited by Witold Brostow. Hanser Publishers,1986.

10. R. W. Hertzberg, J. A. Manson, Fatigue of Engineering Plastics, Academic Press, 1980.

11 G. P. Morgan & I. M. Ward, Polymer, vol.18, p87, 1977.

12 R. Schirrer & M. G. Schinter, Colloid & Pol. Sci., Vol. 259, p812, 1981.

13. R. Talreja, Fatigue of Composite Materials: Damage Mechanisms and Fatigue-Life Digrames, Proc. Soc., London, A378, P461, 1981.

14 H. T.Hahn, "Fatigue Behavior of Composite Laminates," Journal of Composite Materials, Vol. 8, P288, 1974.

15. A. L. Highsmith, "Stiffness Reduction Mechanisms in Composite Laminates," Damage in Composite Materials, ASTM STP 775, P103,1982.

16. K. L.Reifsnider, Fatigue of Composite Materials, Elsevier Science Publishers B.V., Chapters 2-4,1990.

17. J.F.Mandell, "Fatigue Behavior of Short Fiber Composite Materials", Chapter 7, The Fatigue Behavior of Composite Materials, K.L. Reifsnider, Ed., Elsevier Science Publishing, London, 1991.

18 J. F. Mandell, Composite Reliability, ASTM STP 580, ASTM, 1975.

19. M.J. Matthewson, "Fiber Lifetime Predications," Proc. SPIE, Fiber Opt. Compon. Reliability, Vol.1580, 130-41,1991.

20. T.A. Michalske, W.L. Smith, "Fatigure Mechanisms in High-Strength Silica-Glass Fibers," J. Am. Ceram. Soc., Vol.74,1993-96,1991.

21. A.G. Metcalfe, M.E. Gulden, " Propagation of Stress Cracks in Glass Fibers,"Glass Technol. Vol. 12,15,1971.

22. S. M. Weiderhorn, J. Amer. Ceram. Soc. Vol. 50, 543,1970.

23. C. R. Kurkjian and U. C. Paek, "Single-Valued Strength of 'perfect' Silica Fibers," Appl. Phys. Lett., Vol 42, 251-53, 1983.

24. Y. Fujii, A. Murakami, " Study of the Stress Corrosion Cracking of GFRP: Effect of the toughness of the matrix resin on the fatigue damage and stress corrosion cracking of GFRP," J. Material Sci. Vol 29, 4279,1994.

25. Terry A. Michalske, "Steric Effects in Stress Corrosion Fracture of Glass," J. Amer. Ceram. Soc., Vol. 70, 780, 1987.

26. J. F.Mandell, "Fatigue Behaviour of Fiber-Resin Composites.", Developments in Reinforced Plastics, Vol. 2, G. Pritchard, ed. London, Applied Science Publishers, 1982.

27. J. F. Mandell, F. J. McGarry, A. J.-Y. Hsieh, C. G. Li, Polymer Composite, Vol. 6, P 168, 1985.

28. J. F.Mandell, U. Meier. "Effects of Stress Ratio Frequency and Loading Time on the Tensile Fatigue of Glass-Reinforced Epoxy", ASTM-STP, p55, 1983.

29. J.F. Mandell, F.J. McGarry, A.J.Y. Hsieh, "Tensile Fatigue of Glass Fibers and Composites with Conventional and Surface Compressed Fibers," in Proc. 40th Annual Conference Reinforced Plastics/Composites Institute, SPI, Paper 7-G,1985.

30. S. R. Choi, J.E. Ritter, and K. Jakus, "Failure of Glass with Subthershold Flaws," J. Am. Ceram. Soc., Vol. 73, 268, 1990.

31. W. Cheng, E. Ling, and I. Finnie, "Median Cracking of Brittle Solids Due to Scribing with Sharp Indenters," J. Am. Ceram. Soc., Vol. 73, 580, 1990.

32. Weili Cheng, Iain Finnie, " A predication on the Strength of Glass Following the Formation of Subsurface Flaws by Scribing." J. Am. Ceram. Soc., Vol 75, 2565, 1992.

33. Dharan, C. K. H., "Fatigue Failure Mechanisms in a Unidirectionally Reinforced Composite Materials," in Fatigue of Composite Materials, ASTM STP 569, P 171, 1975.

34. Ramesh Talreja, "Fatigue of Composite Materials," Published by Technomic Publishing Company, Inc. P61, 1987.

35. User's Manual, Version 3.0X-TMX 2000 Explorer Atomic Force Microscope. TopoMetrix Co., P8, 1995.

36. Carlo G. Pantano, Interface in Composites, Materials Research Society, 1990.

37. W. P. Hoffman, W. C. Hurley, J. Mat. Sci. Vol.26, 4545, 1991.

38. D. M. Eigler, C. P. Lutz, and W. E. Rudge, Nature, Vol 352, 600, 1989.

39. W. P. Hoffman, " Scanning Probe Microscopy of Carbon Fiber Surfaces," Carbon, Vol.30, 315, 1992.

40. E. P. Plueddemann, Interface in Polymer Matrix Composites, Academic, New York, 1974.

41. Copper, G. A. "Role of the Interface in the Fracture of Fiber-Composite Materials," Interfaces in Composites, ASTM STP Vol. 452, 90, 1969.

42. King-Fu Lin, Shen-Chang Lo, "Surface Treatments of Graphite/Bismaleimide Prepregs and Their Effects on the Properties of Cured Laminates." Composite Material Technology, Vol.53, P199, 1994.

43. K. E. Hofer, Jr., l. C. "Effect of Various Fiber Surface Treatments on The Fatigue Behavior of Glass Fabric Composites in High Humidity Enviroments," SPI, 31st Annual Technical Conference, Section 6-A,Washington, D. C., February 1976.

44. Broutman, L. J., "Measurement of the Fiber-Polymer Matrix Interfacial Strength," Interface in Composites, ASTM STP 452, ASTM, 1969.

45. Bian Jinhua , Zuton Gui, "The Interaction between the Interface of Carbon Black and Polyethylene." Paper for 3rd Asia Pacific Regional Polymer Meeting, P 199, 1992.

46. Chamis, C. C. Composites Materials, Vol. 6, E. P. Plueddemann ed., Academic Press, New York, 1974.

47. A. Terry Michalsk, "A Chemical Kinetics Model for Glass Fracture."J. Am. Ceram, Vol. 76, P2613,1993.

48. J. F. Mandell, D. H. Grande, T. H. Tsiang and F. J. McGarry, " A modified Microdebonding Test for Direct In-Site Fiber/Matrix Bond Strength in Fiber Composites," Composite Materials: Testing and Design, Seventh Conference, ASTM STP 893, P. 87, 1986.

49. D. H. Grande, J. F. Mandell, and K. C. C. Hong, "Fiber/Matrix Bond Strength Studies of Glass, Ceramic and Metal Matrix Composites," Proc. 40th Annual Conference Reinforced Plastics/Composites Institute, Society of the plastic industry, new york, p2,1993.

50. A.Belinky "High Cycle Compressive Fatigue of Unidirectional Glass/Polymer Performed at High Frequency." Master-Degree Thesis, Montana State University, 1994.

51. S. M. Weiderhorn, H. Johnson, A. M. "Fracture of Glass in Vacuum," J. Am. Ceram. Soc., Vol. 57, p36, 1974.

52. Weili Cheng, " A prediction on the Strength of Glass following the Formation of Surface Flaws by Scribing." J. Am. Cerm. Soc., Vol. 75, p2565, 1992.

53. User's Manual, Version 3.0X-TMX 2000 Explorer Atomic Force Microscope. TopoMetrix Co., P26, 1995.

54. Ashby, M. F., "Progress in the Development of Fracture-Mechanism Maps," Fracture, Vol.1, p1, 1977.

55. Tensile Properties of Glass Fiber Strands, Yarns, and Rovings used in Reinforced

Plastics. ASTM 2343, 1985.

56. S. Ochiai, Multiple Cracking of a Coating Layer and Its Influence on Fiber Strength." J. Mater. Sci. Vol. 30, P274,1995.

57. J. F. Mandell, D. D. Huang and F. J. McGarry, Composite Technology Review, Vol.3, P96, 1981.

58 J. F. Mandell & H. J.Sutherland, "High Cycle Tensile and Compressive Fatigue of Glass Fiber-Dominated Composites." ASTM, six Symposium on Composites: Fatigue and Fracture, in Publication.

APPENDIX 1. AFM SCANNING RESULTS FOR FATIGUED FIBERS

SPECIMEN	CRACKS DEPTH (nm)
1	NONE
2	4.5
3	5.4
4	5.8
5	NOT RECORDED
6	NONE
7	6.4
8	6.2
9	NONE
10	NONE
11	4.8
12	5.7
13	NONE
14	6.8
15	NONE
16	6.2
17	4.5
18	NONE
19	5.3
20	NONE
21	4.2
22	NONE
23	NONE
24	4.1
25	6.1

APPENDIX 2. FATIGUE TEST RESULTS FOR GLASS STRAND COMPOSITES

SPECIMEN ID	Maximum Test Stress (S/So)	CYCLES TO FAIL
CONTROL	0.5	152742
	0.5	95876
	0.5	148763
	0.5	124533
	0.5	184326
	0.5	143744
	0.6	5918
	0.6	8924
	0.6	7355
	0.6	6422
	0.6	12472
	0.6	5876
	0.7	1055
	0.7	736
	0.7	984
	0.7	1422
	0.7	1265
AS RECEIVED	0.5	234251
	0.5	102365
	0.5	78695
	0.6	9942
	0.6	2763
	0.6	1997
	0.7	1542
	0.7	828
	0.7	736
COATED	0.5	4669747
	0.5	7605667
	0.5	8754227
	0.5	4275446
	0.5	3898200
	0.6	324635
	0.6	191682
	0.6	194471
	0.6	726944
	0.6	508910
	0.6	730924
	0.7	4382
	0.7	1988
	0.7	2509

0.7	2358
0.7	5388

APPENDIX 3 . FATIGUE TEST RESULTS FOR GLASS FABRIC COMPOSITES

SPECIMEN ID	MAXIMUM STRESS (S/So)	FREQUENCY (Hz)	CYCLES TO FAIL
COATED(B1)	0.4	50	4044156
	0.5	30	399617
	0.5	30	532284
	0.5	30	442073
	0.6	20	9987
	0.6	20	18872
	1.08	20	1
	0.95	20	1
	0.99	20	1
COATED(B 2)	0.25	100	1.1E+8
	0.4	50	832863
	0.4	50	4957470
	0.5	30	367542
	0.5	30	424706
	0.6	20	19446
	0.6	20	35347
	1.09	20	1
	1.01	20	1
	0.95	20	1
AS RECEIVED	0.2	100	1.2 E+7
	0.2	100	1.1 E+7
	0.3	80	927035
	0.3	80	88764
	0.4	50	57230
	0.4	50	16474
	1.08	20	1
	1.03	20	1
	0.95	20	1
DATA BASE	0.21	100	7.9 E+7
	0.21	100	1.1 E+8
	0.21	100	5902329
	0.28	80	2269945
	0.28	80	602984
	0.32	60	702884
	0.32	60	157502
	0.47	20	45845
	0.47	20	2982